Master Thesis

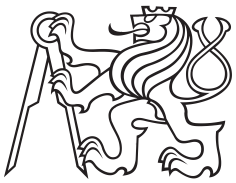

Czech Technical University in Prague

F3

Faculty of Electrical Engineering
Department of Control Engineering

Electric Vehicle Battery Pack State of Charge and State of Health Estimation

Jan Kučera

Supervisor: Ing. David Vošahlík
May 2022

MASTER‘S THESIS ASSIGNMENT

I. Personal and study details

Student's name: **Kučera Jan** Personal ID number: **466186**

Faculty / Institute: **Faculty of Electrical Engineering**

Department / Institute: **Department of Control Engineering**

Study program: **Cybernetics and Robotics**

Branch of study: **Cybernetics and Robotics**

II. Master’s thesis details

Master’s thesis title in English:

EV battery pack State of Charge and State of Health estimation

Master’s thesis title in Czech:

Systém pro odhadování stavu nabytí a kondice baterie elektromobilu

Guidelines:

The goal of this master’s thesis will be to implement model-based algorithms for estimation of vehicle battery pack State of Charge and State of Health. First, the battery pack model parameters will be identified. Parameters, that cannot be measured, will be estimated from real world driving data. Finally, the thesis will present validation of the proposed estimation algorithms.
The thesis will compose of following steps:
1) Get familiar with battery mathematical modeling, state estimation, and degradation models.
2) Measure battery cell physical characteristics. Adopt estimation algorithm and estimate the battery pack parameters from real world driving measurements.
3) Design and implement battery State of Charge estimation.
4) Design and implement battery State of Health estimation.
5) Validate both implemented algorithms.

Bibliography / sources:

[1] Lewis, F. L., L. Xie, D. Popa: Optimal and Robust Estimation: With an Introduction to Stochastic Control Theory, CRC Press, 2005. ISBN 978-1-4200-0829-6
[2] Simon, D.: Optimal State Estimation: Kalman, H Infinity, and Nonlinear Approaches. Wiley, 2006, ISBN: 978-0-471-70858-2
[3] Dieter Schramm, Manfred Hiller, Roberto Bardini – Vehicle Dynamics – Duisburg 2014
[4] Robert Bosch GmbH - Bosch automotive handbook - Plochingen, Germany : Robet Bosch GmbH ; Cambridge, Mass. : Bentley Publishers

Name and workplace of master’s thesis supervisor:

Ing. David Vošahlík Department of Control Engineering FEE

Name and workplace of second master’s thesis supervisor or consultant:

Date of master’s thesis assignment: **28.01.2022** Deadline for master's thesis submission: **20.05.2022**

Assignment valid until:
by the end of summer semester 2022/2023

Ing. David Vošahlík	prof. Ing. Michael Šebek, DrSc.	prof. Mgr. Petr Páta, Ph.D.
Supervisor’s signature	Head of department’s signature	Dean’s signature

III. Assignment receipt

The student acknowledges that the master's thesis is an individual work. The student must produce his thesis without the assistance of others, with the exception of provided consultations. Within the master's thesis, the author must state the names of consultants and include a list of references.

.	
Date of assignment receipt	Student's signature

Acknowledgements

I would like to thank my supervisor Mr. Ing. David Vošahlík who provided me with invaluable support during the work and has always been patient, friendly, and helpful. Also, I would like to thank my manager, Mr. Ing. Jaroslav Pekař, Ph.D., from Garrett Motion company, for allowing me to create this thesis for the company and for a big portion of the trust and freedom he gave me. For the very same attitude, I would like to thank the researchers from the Department of Electrotechnology, FEE CTU in Prague, namely Mr. doc. Ing. Karel Dušek, Ph.D., and Mr. Ing. Pavel Hrzina, Ph.D., for granting me free access to their equipment and also for advice and support. Also, I would like to thank the eForce FEE Prague Formula team members for their help and support. I would like to thank my fellow university friends and colleagues for I would never finish my study being a lone wolf. Special thanks belong to my parents, siblings and other family members who have stood by my side for all the time.

Declaration

I hereby declare that this thesis has been composed solely by myself and that it has not been submitted, in whole or in part, in any previous application for a degree. Except where states otherwise by reference or acknowledgment, the work presented is entirely my own.

Signature:

Prague, May 20, 2022

Abstract

This thesis examines options for state estimation of a battery pack of an electric vehicle. The motivation and the ultimate aim of this work is to improve the battery state estimation capabilities of a student formula race car and help to achieve better results in motorsport competition. This thesis follows the state-of-the-art approach of Extended Kalman Filter. The thesis broadens the scope and presents the whole process of a battery model development, Extended Kalman Filter implementation and validation. A substantial part is dedicated to measurement of model parameters. Then, the other model parameters that were not measured are identified via optimal identification from previously measured data. Successively, the implementation of the Extended Kalman Filter itself is described. Finally, the algorithm is validated using simulation experiments and real driving data. The chosen approach presents itself as a viable, working solution to the problem.

Keywords: State of Charge, State of Health, Extended Kalman Filter, Electric Vehicle, Model-based Design, Battery Capacity, Internal Resistance, Optimal Identification, Equivalent Circuit Model

Supervisor: Ing. David Vošahlík
Department of Control Engineering, FEE CTU in Prague (FEL ČVUT v Praze)
Resslova 9, E-9
12000 Praha 2

Abstrakt

Tato práce zkoumá možnosti odhadování stavu akumulátorového modulu elektrického vozidla. Motivací a konečným cílem této práce je vylepšit schopnost odhadu stavu akumulátoru ve studentské závodní formuli a pomoci dosáhnout lepších soutěžních výsledků. Tato práce implementuje přístup v angličtině známý jako *Extended Kalman Filter*. Ten je v literatuře široce používán. Tato práce rozšiřuje záběr o popis celého procesu vývoje modelu akumulátoru, implementace filtračního algoritmu a validace. Podstatná část je věnována měření parametrů modelu. Následně, neměřitelné parametry jsou identifikovány z předtím naměřených dat pomocí optimální identifikace. Poté je popsána implementace samotného Kalmanova filtru. Na konci je algoritmus zvalidován pomocí počítačových simulací a celá práce je zhodnocena. Zvolený přístup se ukazuje jako funkční řešení daného problému.

Klíčová slova: elektrické vozidlo, stav nabití baterie, stav zdraví baterie, kapacita, vnitřní odpor, Kalmanův filtr, návrh založený na modelu, náhradní model, optimální identifikace

Překlad názvu: Odhad stavu nabití a zdraví akumulátoru elektrického vozidla

Contents

Figures

Tables

Chapter 1

Introduction

Nowadays, we are experiencing a shift towards hybrid, fuel-cell, and electric vehicles in the car industry. There has been a very large amount of studies published about the future of automotive industry. One such prediction is shown in figure 1.1.

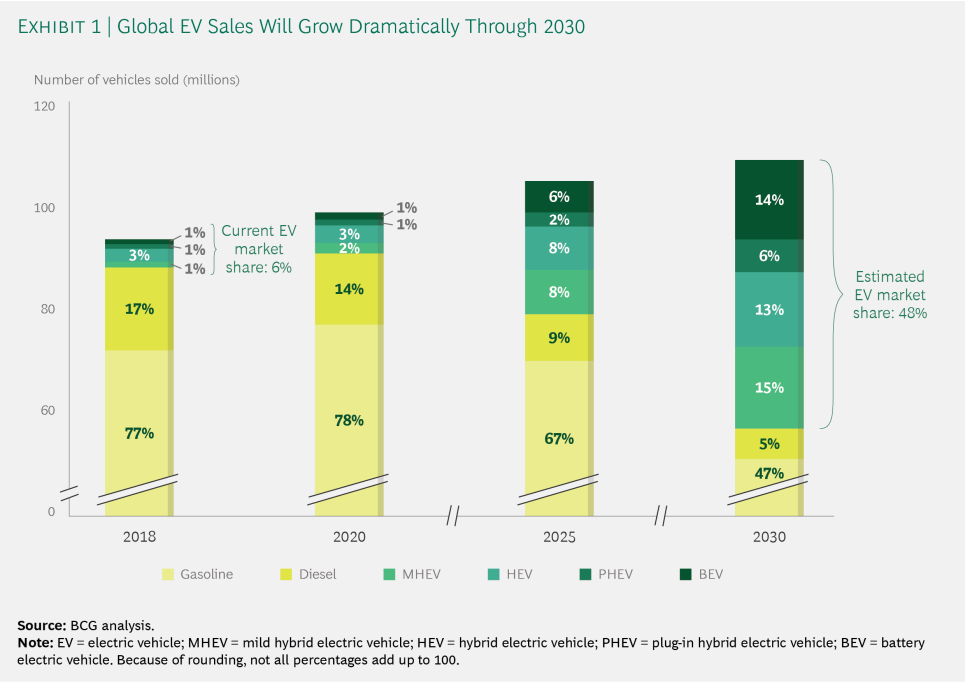

Figure 1.1: BCG analysis on sales of electric vehicles. Source: [Groa]

One of the parts all the electric vehicles have in common is a battery. Moreover, battery technologies are highly sought-after in the power industry, too, with their applications ranging from microgrids to gargantuan battery storage power stations. Their usage can be seen in figure 1.2.

Arguably the most important state of the accumulator system is the State of Charge (SOC). As detailed further in this thesis's text, it is a nontrivial task to determine SOC reliably. This thesis addresses the challenge.

Because the SOC estimation is such a hot topic for both the researchers and the industry players, there is room for mutual collaboration between

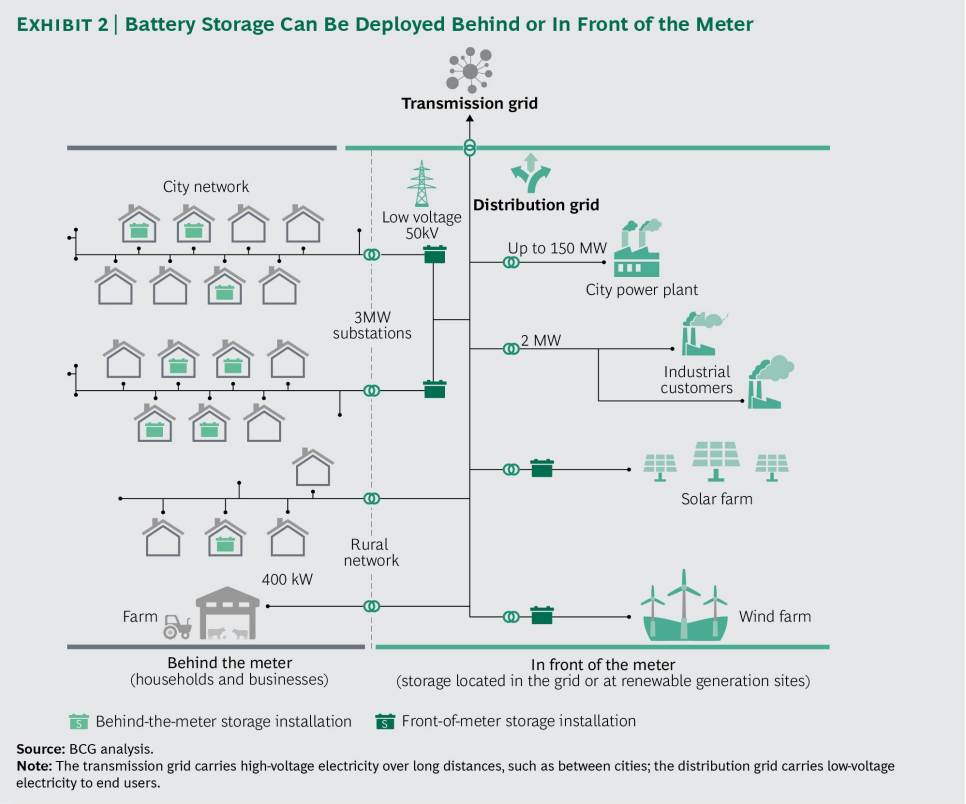

Figure 1.2: BCG analysis on battery usage in power grid. Source: [Grob]

companies and schools. This thesis embodies such a symbiosis since it was created for Garrett Motion company in order to foster its activities in the field. Parts of code developed for the purpose of this thesis are used in the company's proprietary framework. Namely, the company's framework was augmented with the estimation algorithm. On the other hand, the optimal identification tool that was used for model fitting had already been a part of the framework before.

Furthermore, this work is motivated not only by research interests or industrial aims but also by a motorsport application. The ultimate goal is to use the algorithm in a small formula-type race car. Thus, the development is being done with a future embedded application in mind.

The work is divided into several steps. After this introductory part, there is a chapter devoted to batteries and their models. After that, an overview of other approaches to the problem is presented. Then, the estimation algorithm is chosen and implemented. Then, the algorithm is tested and evaluated. Finally, results are assessed and discussed.

1.1 Formula Student

Formula Student is an engineering students' competition. The aim is to design and develop a formula-style car and take part in a competition. Formula

Student originated in the United States and spread worldwide. The author of this thesis is a member of the eForce FEE Prague Formula team, which develops a fully electric race car for the purpose of the Formula Student competition.

	CV & EV	DC
Static Events:		
Business Plan Presentation	75 points	-
Cost and Manufacturing	100 points	-
Engineering Design	150 points	150 points
Dynamic Events:		
Skid Pad	50 points	-
DV Skid Pad	75 points	75 points
Acceleration	50 points	-
DV Acceleration	75 points	75 points
Autocross	100 points	-
DV Autocross	-	100 points
Endurance	250 points	-
Efficiency	75 points	-
Trackdrive	-	200 points
Overall	1000 points	600 points

Table 1.1: Formula Student Germany 2022 Events & Score

The Formula Student competition events consist of several disciplines which are awarded with points. For example, the Formula Student Germany 2022 disciplines and respective points are shown in table 1.1. The abbreviations used in the table mean: CV - combustion vehicle, EV - electric vehicle, DC - driverless cup, and DV - driverless vehicle. The CV and EV vehicles compete in the same categories, plus, provided they are equipped with autonomous systems, they can take part in the Driverless Cup. All the points add up together, and the team with the highest score wins. Taking the static events aside (they cover the business and design part of a formula car development), there remain dynamic events that make up the bigger portion of points. The Skid Pad examines the lateral acceleration of the vehicle. It is a race on an 8-like shaped track. The Acceleration is done on a 75 meters long, straight track. The Autocross track is a loop with straights, various kinds of turns, slaloms, etc. The length of the Autocross is 1.5 km. The Trackdrive is the same track as in Autocross. Then, there is Endurance & Efficiency. The track also comprises straights, various turns, slaloms, chicanes, etc. However, the length of one lap is approximately 1 km, and the length of the complete endurance is ca. 22 km.

In conclusion, the endurance event is the single event where reliable SOC estimation (or, in fact, range estimation) is absolutely crucial. It is also the single most rated event. Moreover, it is vital to know the exact amount of energy consumed during driving when the team wants to improve its efficiency score. The Endurance & Efficiency make up together 325 points which might

be a third of all available points if the team does not aspire to compete in the Driverless Cup. Thus, a proper SOC estimation can improve teams' results significantly.

Chapter 2
Battery Modelling

In this section, a brief introduction to *lithium-ion* (li-ion) batteries is treated and then a battery model is devised. This model will be used later in the estimation algorithm. Other approaches to SOC and SOH estimation are presented in the next chapter.

The field of battery modeling is vast. Not only is there a huge amount of approaches and techniques, but the spectrum of battery chemistries adds up complexity, too.

A deep insight into all phenomena occurring in the battery is beyond the scope of this thesis. This section aims to provide an introductory overview of the operation and properties of Li-ion batteries.

2.1 Li-ion Batteries

The li-ion batteries are widely used across various industries today. They are the so-called *secondary batteries* which are, as opposed to the *primary batteries*, rechargeable (even multiple times). Their highlight features are (relatively to other battery technologies): high energy density, high voltage, long cycle life, low self-discharge, and wide operating conditions [Bea19].

Charging and discharging mechanisms are shown in figure 2.1. Lithium ions travel back and forth in the battery between the electrodes while electrons travel in the outer circuit.

2.2 State of Charge Background

Even the definition of SOC itself is a matter of dispute. According to [LHLZ17], taking the underlying physical principles into account, the SOC could be described as a state of thermodynamic equilibrium. However, instead of resorting to thermodynamics and statistical physics, an (alternative) empirical approach is taken in this thesis.

In this thesis, SOC [%] is a ratio of a current charge present in the battery Q_{cur} to the actual maximum available capacity of the battery Q_{max} ([HHA22]):

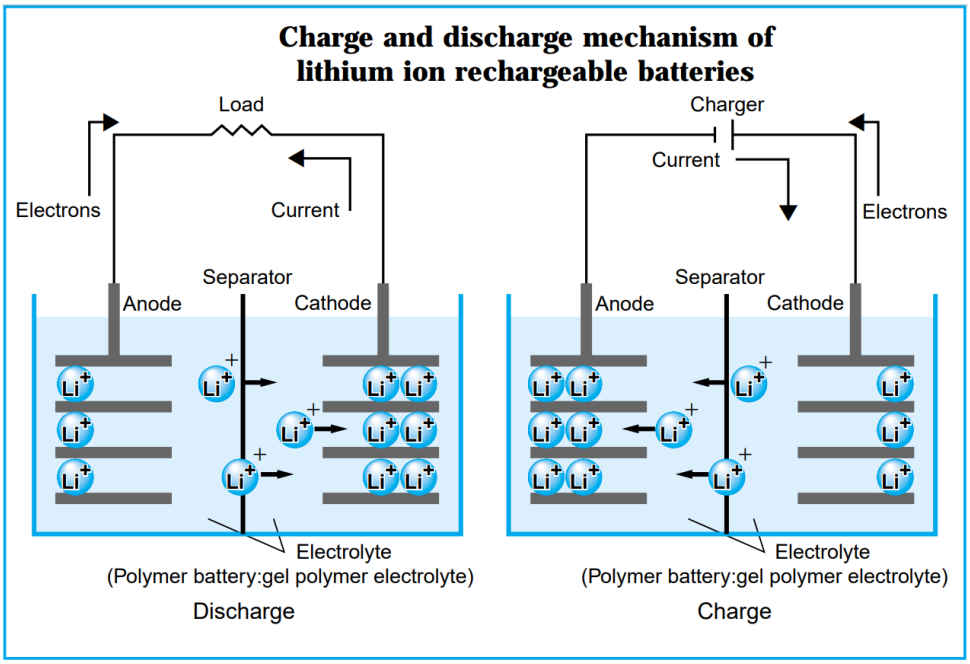

Figure 2.1: Charge and discharge of a Li-ion battery. Source: [Son]

$$SOC = \frac{Q_{\text{cur}}}{Q_{\text{max}}} \cdot 100\,. \tag{2.1}$$

The advantage of such an approach is that: 1) it allows for a much simpler mathematical apparatus to be used, 2) techniques for SOC laboratory determination are much simpler and more easily accessible, 3) it is a concept widely used in literature - it clearly works.

However, the actual maximum available capacity of the battery Q_{max} is not constant, quite the contrary. For example, it can be modelled as a function of two variables - number of cycles n and temperature T, $Q_{\text{max}} = f(n, T)$. That means, in fact, that according to this definition, SOC lowers, for example, in the case when the battery warms up (due to weather conditions), and its maximum rated capacitance increases even though no current has been sunk from the battery. However, these technicalities are of no significance for the end-user as range estimation is an engineering problem on its own. It is a range estimation systems' responsibility to provide useful data to the end-user, and it is out of the scope of this thesis.

The main problem of SOC is that it cannot be measured directly. That is the reason why estimation is necessary.

2.3 State of Health Background

Defining *State of Health* (SOH) is more involved than defining SOC. As described in [YXT+21], there are multiple phenomena occurring in the cell,

as depicted in figure 2.2. However, as a result, all these processes have an impact on two key cell parameters - capacity and internal resistance. The SOH [%] is given as a ratio of the actual maximum available capacity to the initial maximum capacity ([YXT+21], [TKP15]):

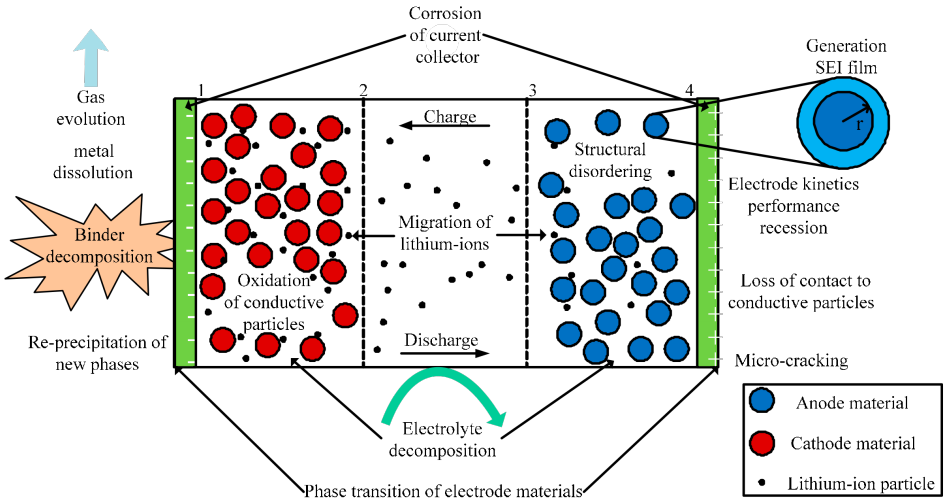

Figure 2.2: Cell aging mechanisms. Source: [YXT+21]

$$SOH_C = \frac{Q_{\max}}{Q_{\text{init}}} \cdot 100\,. \tag{2.2}$$

However, the article [jLhPK16] uses an alternative definition with Q_{end} denoting the capacity the cell has at the end of its life:

$$SOH_C = \frac{Q_{\text{cur}} - Q_{\text{end}}}{Q_{\text{init}} - Q_{\text{end}}}\,. \tag{2.3}$$

Furthermore, the SOH can be defined by resistances, e. g. in [jLhPK16] or in [YXT+21] (with inverse signs) the definition is

$$SOH_R = \frac{R_{\text{cur}} - R_{\text{end}}}{R_{\text{init}} - R_{\text{end}}}\,. \tag{2.4}$$

This thesis uses equation 2.2 as an exclusive SOH definition. The cell degradation through the increase of the internal resistance is not taken into account in this thesis.

2.4 State of the Art - Battery Models

According to [Bea19], there are two classes of battery models, *empirical* and *mechanistic*. Alternatively, a comparative study [HLP12] uses the categories

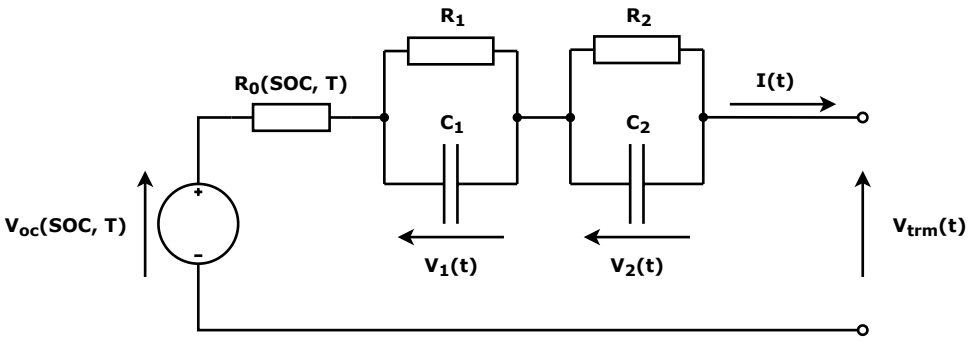

Figure 2.3: Equivalent circuit model of battery cell

equivalent circuit models and *electrochemical models*. These two divisions are in accordance with each other. The principle is that the mechanistic or electrochemical models describe (by means of differential equations) electrochemical procedures that happen in the cell. On the other hand, the empirical or equivalent circuit models make use of structures that do not reflect the battery guts. Instead, they link operating conditions and measured quantities into a model corresponding to the observed battery behavior.

What model to use depends, naturally, on the target application. The electrochemical models provide better accuracy at a higher computational cost. It has been shown in the literature, for example, in [BSM+20, YHjX15, LHLZ17], in the series of articles [Ple04a, Ple04b, Ple04c, Ple06a, Ple06b] and further in [JZK18, HLP12, YXL17], that equivalent circuit models provide a sweet spot of both acceptable accuracy, complexity, and computational effort. In accordance with development previously done within the industrial partner of this work, Garrett Motion company, the 2RC model has been chosen for the purpose of this thesis. Other options could be, for example, the 1RC model, the 3RC model, the Randles model, the one-state hysteresis model... [HLP12].

2.5 Identification Model

The schematic of the equivalent circuit that models the battery is shown in figure 2.3. It comprises a voltage source V_{OC} (regarded as the source of the *Open Circuit Voltage*, OCV), an internal resistance R_0, two RC elements, and output terminals.

Generally, the states' derivatives are given as a function of model states $x(t)$ that explicitly depend on time, inputs $u(t)$ that depend on time likewise, parameters $\mu(...)$ that depend on other quantities than time, and parameters θ that are assumed to remain constant:

$$\dot{x} = f(x(t),\, u(t),\, \mu(...),\, \theta)\,. \tag{2.5}$$

The following equations and tables describe the mathematical relations in the model in detail. The state equation 2.6,

$$\begin{bmatrix} \dot{SOC}(t) \\ \dot{V}_1(t) \\ \dot{V}_2(t) \\ \dot{T}_{\text{bat}}(t) \end{bmatrix} = \begin{bmatrix} -\dfrac{I(t)}{\text{Q}_{\text{max}}} \\ \dfrac{I(t)}{\text{C}_1} - \dfrac{V_1(t)}{\text{R}_1\text{C}_1} \\ \dfrac{I(t)}{\text{C}_2} - \dfrac{V_2(t)}{\text{R}_2\text{C}_2} \\ \dfrac{V_1(t)I(t)}{\text{C}_{\text{th}}} + \dfrac{V_2(t)I(t)}{\text{C}_{\text{th}}} + \dfrac{R_0(SOC,\, T_{\text{bat}})I(t)^2}{\text{C}_{\text{th}}} + \dfrac{T_{\text{air}}(t) - T_{\text{bat}}(t)}{\text{R}_{\text{th}}\,\text{C}_{\text{th}}} \end{bmatrix}, \tag{2.6}$$

is a full realization of the equation 2.5 and prescribes computation of time derivatives of the system states. The states are described in table 2.1.

State name	Unit
State of Charge SOC	Percents %
Voltage V_1	Volts V
Voltage V_2	Volts V
Temperature T_{bat}	Degrees Celsius °C

Table 2.1: System states

The inputs are stated in equation 2.7,

$$u(t) = \begin{bmatrix} I(t) \\ T_{\text{air}}(t) \end{bmatrix}, \tag{2.7}$$

and described in table 2.2.

Input name	Unit
Battery terminal current I	Amperes A
Battery temperature T_{bat}	Degrees Celsius °C

Table 2.2: System inputs

The $\mu(...)$ parameters are represented by the following nonlinear dependencies of the internal resistance R_0 (2.8) and V_{OC} (2.9),

$$R_0 = f_{R0}(SOC,\, T)\,, \tag{2.8}$$
$$V_{\text{OC}} = f_{\text{VOC}}(SOC,\, T)\,. \tag{2.9}$$

Both are obtained by experimental measurements and stored in the form of look-up tables.

Parameter name	Unit
Resistance R_1	Ohms Ω
Capacitance C_1	Farads F
Resistance R_2	Ohms Ω
Capacitance C_2	Farads F
Thermal resistance R_{th}	Kelvin/Watt K/W
Thermal capacitance C_{th}	kilojoule/Kelvin kJ/K
Maximum available battery capacity Q_{max}	Ampere hours $A\,h$

Table 2.3: Constant parameters

The last element in the function in equation 2.5 are the constant parameters θ. Their description can be found in table 2.3.

Now the last thing that needs to be introduced are the system outputs $y(t)$,

$$y(t) = \begin{bmatrix} SOC \\ V_{\text{trm}} \\ T_{\text{bat}} \end{bmatrix}, \tag{2.10}$$

where V_{trm} is the battery terminal voltage,

$$V_{\text{trm}} = V_{\text{OC}} - V_2 - V_1 - R_0 I\,. \tag{2.11}$$

A question arises - how to obtain all the model parameters? Two means can be utilized, either measurement or identification from gathered data. The task was split into these two as follows: the $\mu(...)$ parameters have been measured, and the θ parameters have been determined through least-squares optimal identification.

The SOC can be taken as measured thanks to the SOC estimation method currently used in the car. This is described in other section. The aforementioned model serves well for parameter identification. Nevertheless, it is not suited for SOH estimation, and it moreover uses the SOC estimation algorithm we want to replace. Because of that, later in this thesis, the model will be modified.

2.6 Model Parameter Measurement

Experiments were arranged in order to measure the $\mu(...)$ parameters. An underlying assumption was made that these measured parameters would be easily scalable for various configurations of cells. That, for example, the open-circuit voltage and the state of charge (V_{OC} - SOC) dependence will hold even for a battery pack, and it will suffice to simply multiply the curve by the number of cells in series. Put another way, there is an assumption of a neglectable cell-to-cell variation among their characteristics.

The first type of experiment aimed at obtaining the open circuit voltage V_{OC} and internal resistance R_0 dependencies on state of charge SOC and temperature T_{bat}.

To obtain the V_{OC} at some point of SOC, all that needs to be done is to wait sufficiently long for the transients (modeled by the RC elements in 2.3) to cease away. What does it mean to wait sufficiently long? An experiment was done to get to know (described below).

Unlike the V_{OC}, it is hard to measure the internal resistance. There are three methods available - *DC load*, *AC load*, and *Electrochemical Impedance Spectroscopy* (EIS). The EIS is the richest one in the information provided, yet the most difficult one to be made working. The DC and AC load methods both provide different yet correct results because the cell impedance is frequency-dependent. For the purpose of this thesis, the DC load method was chosen not only because of the relatively easiest implementation and least instrumentation requirements, but it can also be justified by looking at figure 2.4. There, the battery pack terminal current measured during a Formula Student racing event was taken and underwent the Fast Fourier Transform (FFT). Clearly, as the current is directly dependent on a human pilot controlling a pedal, the frequencies are low.

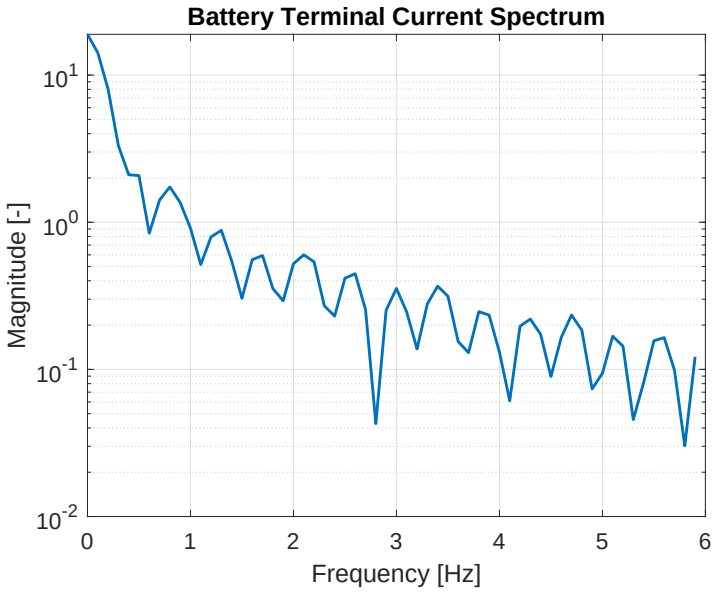

Figure 2.4: FFT of Battery Terminal Current

2.6.1 Measurement setup

A measurement setup schematic can be seen in figure 2.7. There are two pictures of the setup, too - 2.5 and 2.6. The setup consists of a thermal chamber, battery cell, electronic DC source, electronic DC load, relay, and a microcontroller kit STM32 F103 NUCLEO from STMicroelectronics. Furthermore, the source is connected to the PC via GPIB-to-USB. The load and

the microcontroller are both connected via simple USB-USB cables.

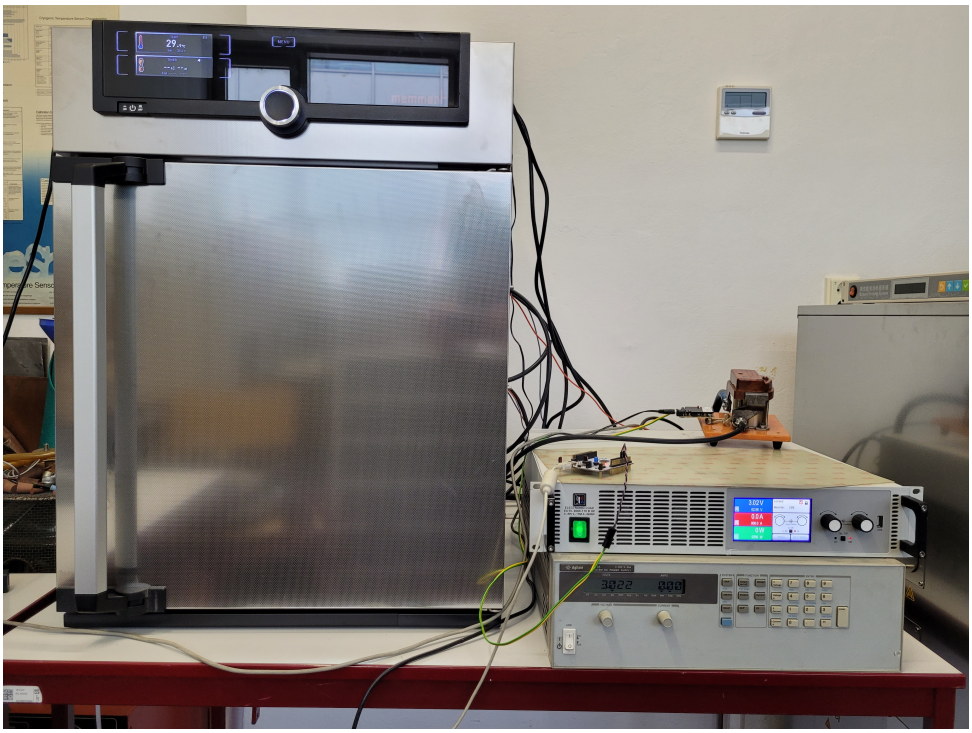

Figure 2.5: General look of the measurement setup

Figure 2.6: Inside the thermal chamber

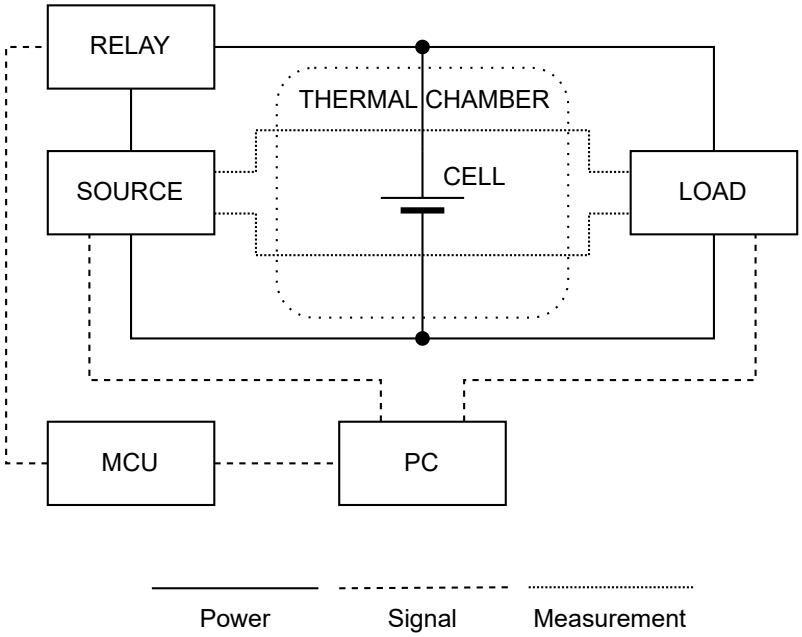

Figure 2.7: Measurement setup

Both the source and the load can be used for voltage and current measurements, providing that both are capable of four-wire measurements. However, different source and load behavior were observed during the switch-off state. While the output terminals of the load have a large resistance between them when switched off (over 20 MΩ), the output terminals of the source have a very small resistance (less than 1 Ω). That means the circuit becomes alive and starts conducting immediately when the cell is connected to the source output, which is totally undesirable. The first attempt to overcome this issue was to connect the cell and the source in series. However, the source and the load interfered with each other, and the measurement was spoiled. The load was not able to regulate its output to zero voltage drop. So in the second step, the issue has been solved by using a relay that disconnects the source from the cell, as shown in figure 2.7.

The load type is EA EL 9080 170 B HP [Ele19]. It can sink up to 170 A and 2400 W, which is more than enough for single-cell testing. Also, the maximum connected voltage is 80 V. The key parameters are summarized in table 2.4.

The display error adds to the error of the set value.

The source type is Keysight (Agilent) 6673A [Key14].

The figure 2.8 depicts how the cell electrodes and power cables from the instrumentation are connected and mounted together. A little hole was drilled through the cell electrodes. The power cables are ended with eyelets. The two eyelets and the electrode are tightened together by a 3 mm bolt and a nut, both supported by washers. In the left part of the picture, a crocodile clip of the four-wire measurement cables can be seen.

The connection through eyelets proved to be very effective. Connection

Parameter	Value
Maximum input voltage U_{max}	80 V
Maximum input power P_{max}	2400 W
Maximum input current I_{max}	170 A
Set voltage accuracy	<= 0.1% U_{max}
Voltage display accuracy	<= 0.1%
Set current accuracy	<= 0.2% I_{max}
Current display accuracy	<= 0.1%
Voltage resolution	0.01 V
Current resolution	0.1 A

Table 2.4: Load key parameters

Parameter	Value
Maximum output voltage	35 V
Maximum output current	60 A
Set voltage accuracy	0.04% + 35 mV
Set current accuracy	0.1% + 40 mA
Voltage readback accuracy	0.05% + 50 mV
Current readback accuracy	0.1% + 60 mA
Voltage resolution	10 mV
Current resolution	15 mA

Table 2.5: Source key parameters

resistance was measured at several places in the setup by Gossen Metrawatt METRAHIT 27I ohmmeter. The values range from 0.02 mΩ to 0.11 mΩ. For example, the resistance between the upper eyelet in 2.8 and the electrode is 0.05 mΩ and the resistance between the electrode and the lower eyelet is 0.04 mΩ.

2.6.2 Measurement Software

To control all the devices, a program in Python language was written. Both the source and the load support VISA commands. The F103 kit was programmed via MBED Compiler, and it only receives 0 or 1 through serial communication and sets its GPIO to high or low accordingly to connect or disconnect the relay. The Python software controls the devices and collects measured data, and stores it in CSV (comma-separated value) format.

2.6.3 V_{OC}, R_0 Measurement Procedure

The DC load measurement method is partly inspired by [Key17] and as the main resource served norm [Com14].

Figure 2.9 shows that typically, the currents drawn from the battery pack during the Formula Student Endurance Event range up to 60 A. Thus, let this

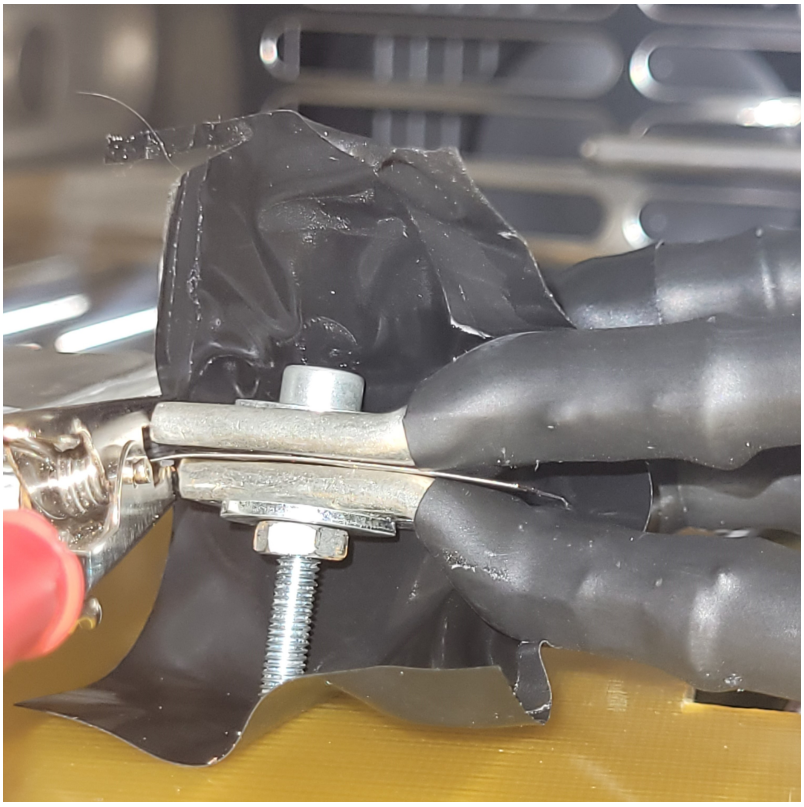

Figure 2.8: Cell mounting

histogram be a supporting justification for the magnitude of the discharge current pulse stated below.

Firstly, it is necessary to measure cell capacity at the actual temperature. The cell is discharged to its cutoff voltage, 3.0 V. The rate of discharge is 30 A, which is approximately 4.3 C (C-rate is a unit of current given as a multiple of battery capacity specified in ampere-hours), which is comfortably below the maximum continuous discharge current of 105 A (15 C) as specified in [She19]. For most of the voltage range, the load works in *constant current* mode - the current remains constant, and the voltage of the cell decreases. However, on the point of reaching the cutoff voltage, the load switches to *constant voltage* mode - cell voltage remains the same while current decreases. Discharge is stopped when the current is equal to or less than 100 mA. This value was chosen with respect to the measurement precision of the load. It was observed that when the discharge task is done, and the cell is left to rest, its voltage starts to increase immediately, even to a value of roughly 3.1 V within a few minutes. That means the load is not able to bring the V_{OC} to 3.0 V within one discharge routine. To get the V_{OC} closer to 3.0 V, the discharge routine is repeated after five minutes' rest.

Subsequently, the cell is charged with 7 A (1 C), again far below the maximum specified continuous charge current of 14 A (2 C). These values were chosen as a sweet spot regarding the prevention of excessive heating and cell

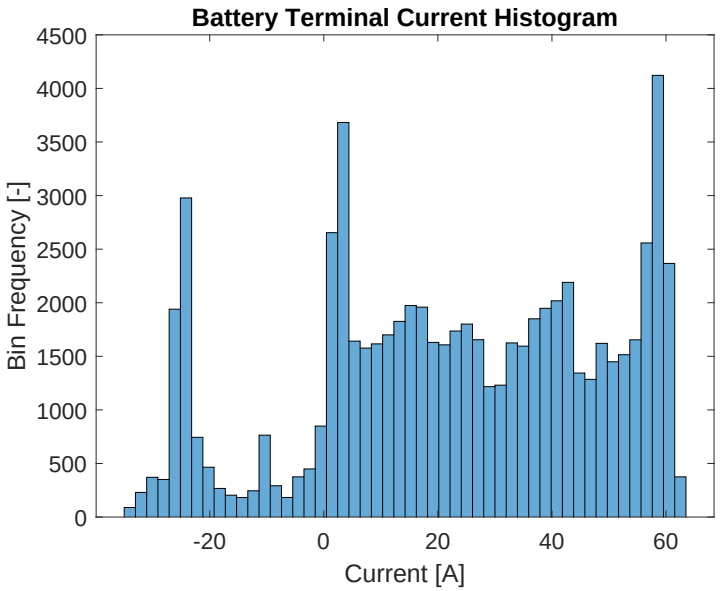

Figure 2.9: Histogram of currents drawn from the battery pack

damage on the one hand and the duration of the experiment on the other hand. Analogously to the discharge routine, charging is done three times with five minutes' rest to approach the true V_{OC} of 4.2 V. Then, the value of charge infused into the cell is stored so that the value of charge corresponding to 100% SOC is known.

In the next step, the course of measurement keeps on gradually descending (discharging) from 100% to 0% (for example, equally divided into 4% steps as in the first measurement) and carries out the open-circuit voltage and internal resistance measurement at each point.

2.6.4 First Measurement

The aim of the first measurement was to get to know how long it is necessary to wait for the OCV to settle and also if the measurement can provide meaningful results. Starting at 100% of SOC, a discharge procedure was carried out, and at 96%, 48%, and 0% of SOC, the algorithm waited for ninety minutes and read the voltage value every five minutes. The result is shown in figure 2.10.

It can be seen that at 96% of SOC, the terminal voltage V_{trm} reaches the V_{OC} right after 10 minutes of resting. At 48% of SOC, the terminal voltage V_{trm} reaches the V_{OC} after 35 minutes of resting. In the last case, the V_{OC} is reached after 70 minutes.

Two possible explanations for these differing settling times were considered. 1) It could be a natural cell property, dependent only on the V_{OC}. 2) It could be highly influenced by skipping the resting after each measurement procedure.

It is impractical to wait for 70 minutes to get the V_{OC}. Because of that,

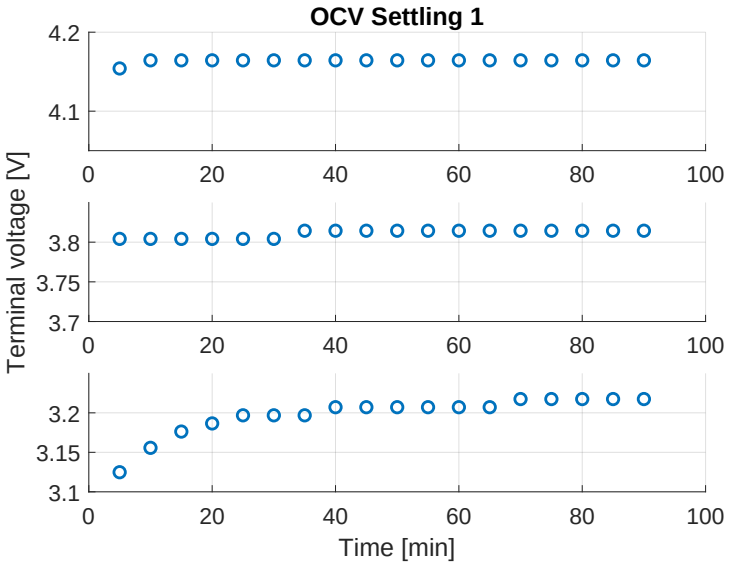

Figure 2.10: V_{OC} Settling during the first measurement

another experiment was necessary to further investigate this behavior.

As a second result of the first measurement, the dependence of the internal resistance on SOC was measured. It can be seen in 2.11. Strictly speaking, as the measurement went from 100% SOC to 0%, the dependence of the internal resistance on the so-called *Depth of Discharge*, DOD, was measured,

$$DOD = 100 - SOC. \tag{2.12}$$

Measured resistances are stratified into four levels. This could be due to the low current measurement resolution of the used load. The mean value is 2.28 mΩ. Thus, the maximum value in the data set is 118.6% of the mean, and the minimum value is 91.2% of the mean.

2.6.5 Second Measurement

In the second measurement, the cell was discharged in steps 4% as in the first measurement (at room temperature). At each point, there was a rest of 20 minutes with voltage measurements every 5 minutes. The aim was to check if 20 minutes' rest is enough for the V_{OC} to settle if the resting is carried out at every SOC point of the measurement procedure. The results are shown in table 2.6 (not all the values are shown for brevity).

It is clear that 20 minutes are enough for the V_{OC} to settle down. Only the last row in the table shows that at low SOC values, the V_{OC} would need more time to settle. The system dynamics in this region are highly nonlinear and noisy (SOC equals 0.5%), and thus, there is no practical significance in waiting for the V_{OC} to settle completely.

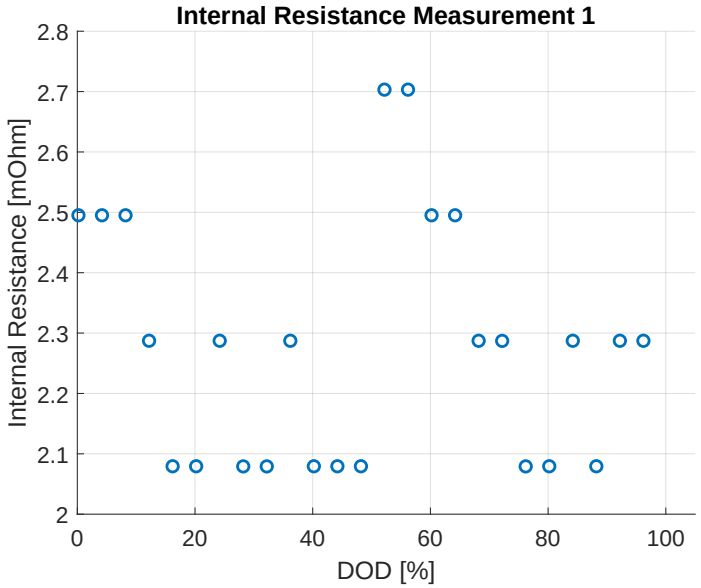

Figure 2.11: Internal Resistance Measurement 1

Settling time [min]	5	10	15	20
96% SOC	4.15 V	4.15 V	4.16 V	4.16 V
76% SOC	3.97 V	3.97 V	3.97 V	3.97 V
56% SOC	3.85 V	3.85 V	3.85 V	3.85 V
36% SOC	3.77 V	3.77 V	3.78 V	3.78 V
16% SOC	3.71 V	3.72 V	3.72 V	3.72 V
4% SOC	3.56 V	3.56 V	3.56 V	3.56 V
0.5% SOC	3.09 V	3.11 V	3.12 V	3.14 V

Table 2.6: Open circuit voltage V_{OC} settling

The figure 2.12 reveals the V_{OC} - SOC dependence. It is aligned with curves seen in the literature. These data are fit for polynomial fitting and usable for the cell model.

On the contrary, the internal resistance measurement is unsatisfactory. Although at least from 2.13 some trend towards increasing internal resistance in lower SOC could be derived, from both the 2.11 and 2.13 figures, it is clear that the measurement cannot be made with sufficient accuracy. The reason is the resolution of the electronic load.

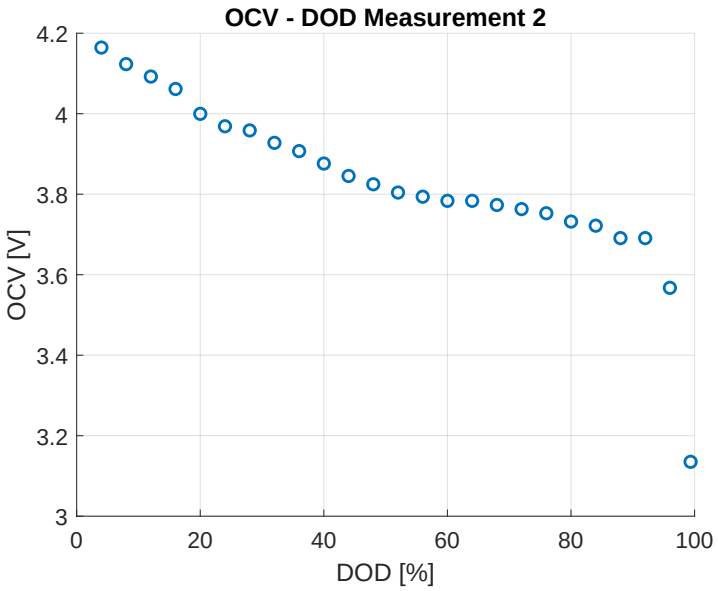

Figure 2.12: V_{OC} - SOC dependence, Measurement 2, room temperature

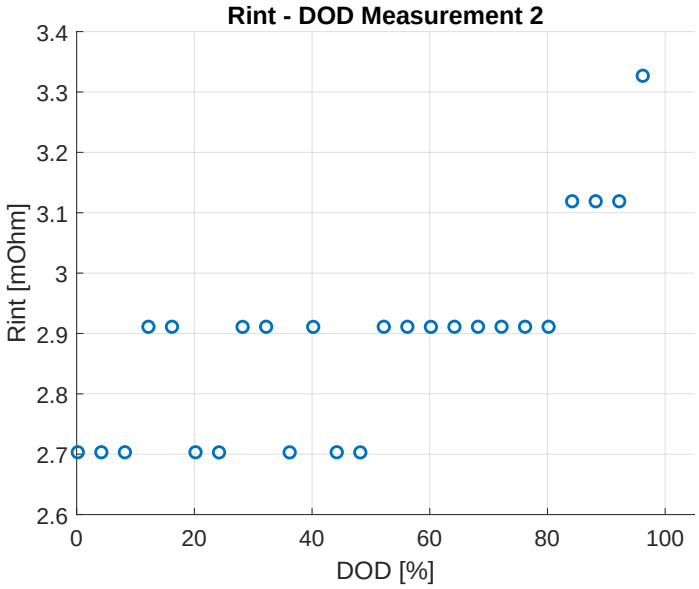

Figure 2.13: Internal resistance - DOD dependence, Measurement 2, room temperature

2.6.6 Final Measurement

After making several adjustments and bug fixes to the measurement procedure, complete results were obtained. They are shown in figures 2.14 and 2.15.

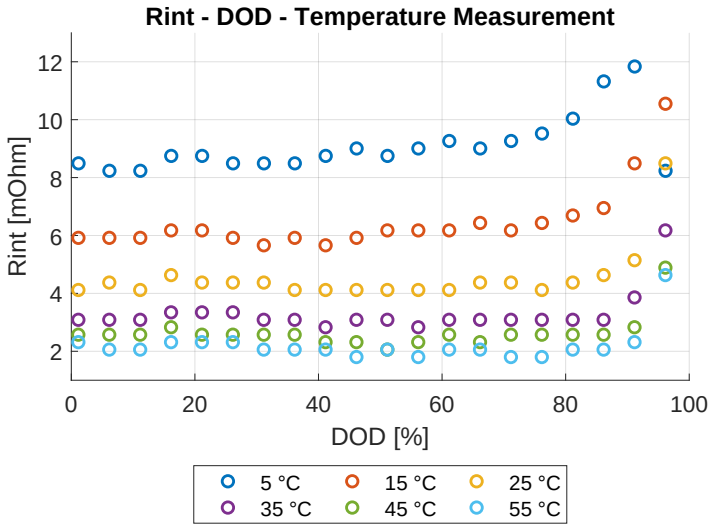

Figure 2.14: Internal resistance - DOD - Temperature dependence

In 2.14, it can be seen that cell temperature clearly influences the internal resistance. Also, the internal resistance steeply increases in lower SOC.

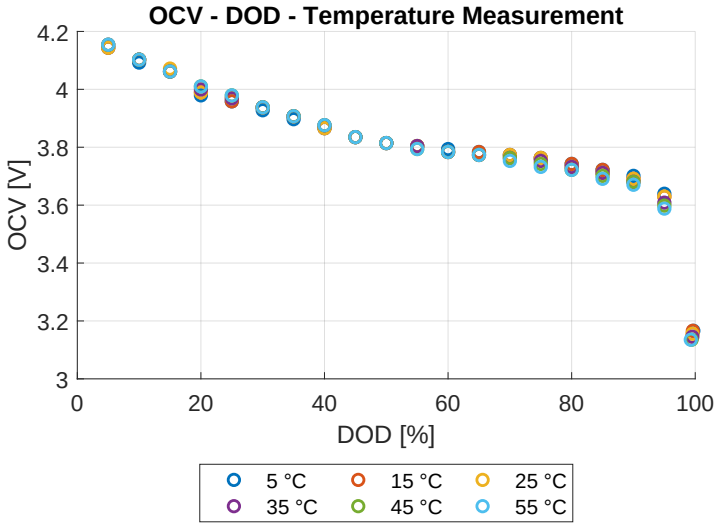

Figure 2.15: V_{OC} - DOD - Temperature dependence

On the other hand, the temperature does not have any major impact on the V_{OC} characteristic. Only in the regions of 75 - 80% and then under 30%.

Whether the measurement was successful or not will be evaluated according to the fitting of the model to the measured formula car data.

2.7 Optimal Identification

As mentioned previously, the way of obtaining the remaining model parameters is their identification from experimental data. In this case, the Formula Student Endurance event data were used.

At this point, an important transition happened. The measurements described in the previous section were carried out with a single cell. But now, the data were scaled appropriately according to the configuration of cells in the battery pack in the formula car. So the optimal identification described below identified model parameters for the whole battery pack, which was modeled as the same 2RC structure as in 2.3.

The data were divided into two sets: training and test. For the purpose of identification, the three-output model 2.10 was used. That means the data provided by the previously used SOC estimation algorithm are utilized in the process.

2.7.1 Implementation

The identification was made within a proprietary tool from the Garrett Motion company. In its core, the tool uses the `fmincon` function of MATLAB®. It is suited for solving optimization problems with nonlinear constraints.

The optimization problem states as follows: a sum of squared differences between observed system output y^{D} (data) and model output y^{M} for each sample of the training data signal of length N must be minimized,

$$\min \sum_{i=1}^{N} \left(y_i^{\mathrm{D}} - y_i^{\mathrm{M}} \right)^2 . \tag{2.13}$$

subject to constraints imposed on y^{M} by equations 2.6 and 2.10 and equality/inequality constraints on the constant parameters θ that can be seen in table 2.7.

Parameter	Initial value	Minimum	Maximum
Resistance R_1	30 mΩ	1 mΩ	200 mΩ
Capacitance C_1	100 F	25 F	400 F
Resistance R_2	60 mΩ	1 mΩ	200 mΩ
Capacitance C_2	10 F	2.5 F	40 F
Thermal resistance R_{th}	50 K/W	1 K/W	100 K/W
Thermal capacitance C_{th}	25 kJ/K	15 kJ/K	35 kJ/K

Table 2.7: Parameter constraints for identification

During the work, it showed up that it is important to scale the model parameters properly. Otherwise, one may end up in a situation where the optimized parameter is completely insensitive to any perturbations induced by the optimizer. In case some parameter is completely unknown, the

identification tool enabled fixing the other parameters and tuning only a single one which sped up the computation and facilitated finding a reasonable range of values for the optimizer to start with.

2.8 Results

An example of a result of the optimal identification can be observed in figure 2.16. More precisely, there is a result of validating an identified model. The model parameters are shown in table 2.8.

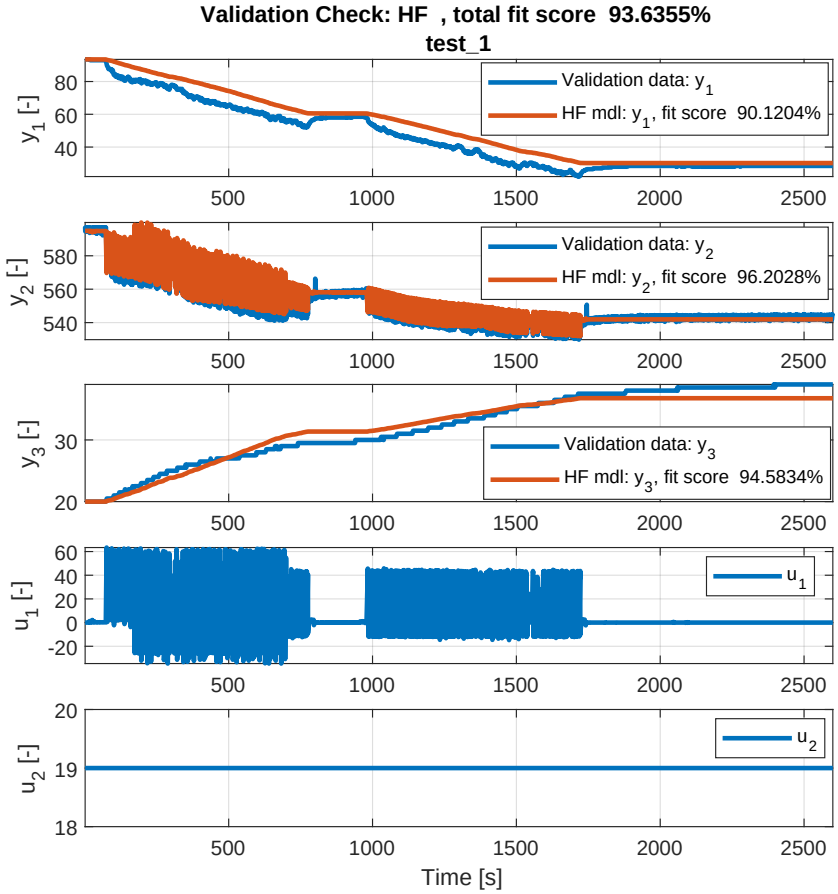

Figure 2.16: Validation of identified model

Through the course of the work, several other models were identified, but they emerged as unsuitable. For example, the first identified model had time constants of 3.6 ms and 7.6 ms. Such time constants are problematic in multiple aspects. Firstly, they are even shorter than the period of the control program in the car, that is 10 ms. Secondly, they are very close to each other, which caused observability issues (unobservable system made the implemented filter to diverge) - it arose necessary to have the time constants further from each other. Thirdly, they do not capture the behavior the users

Parameter	Value
Resistance R_1	36 mΩ
Capacitance C_1	251 F
Resistance R_2	21 mΩ
Capacitance C_2	20 F
Thermal resistance R_{th}	50 K/W
Thermal capacitance C_{th}	25 kJ/K

Table 2.8: Identified model parameters

want to grasp. This can be seen in a quick glimpse back to figure 2.4 again. Inferring from the prospective real-world application, it can be stated that the faster dynamic should be able to cover pressing the accelerator pedal by the pilot. The slower dynamic should encompass the battery behavior on a horizon from lower tens of seconds to lower tens of minutes.

2.9 Aging Experiment

An experiment was carried out to obtain battery capacity degradation data. A cell (other than that one used in the previous experiments) was connected in the same setup as already described earlier in the text. The cell was kept at 30 °C in a thermal chamber, discharged with 35 A constant current (changing to a constant voltage regime at the end). The charging current was 10.5 A. The cell underwent 180 cycles. The results are depicted in figure 2.17 It is to be noted that the manufacturer of the cell declares preserving at least 80% of the initial capacity after 100 cycles. However, in this experiment, the cell preserved roughly 98.5% of its initial capacity after 180 cycles.

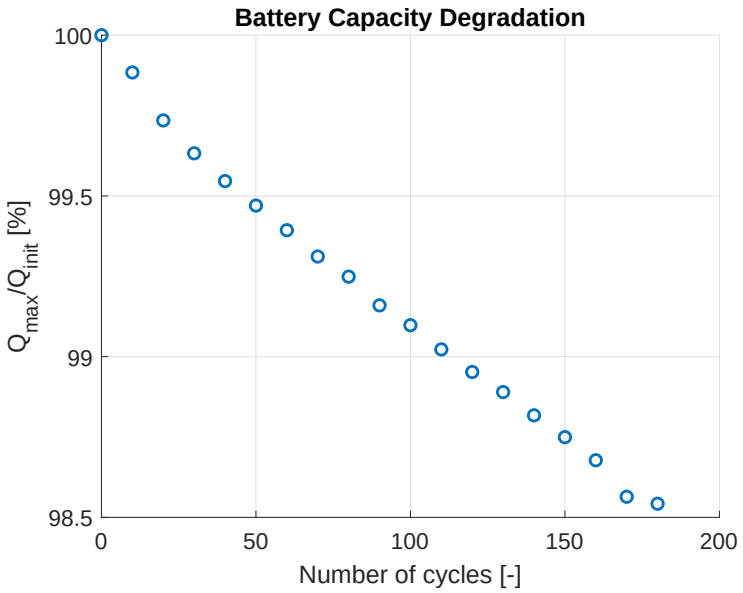

Figure 2.17: Degradation Experimental Data

2.10 Application Model

As it has been noted already, previously measured SOC data were used for model identification. Nevertheless, such kind of information will not be available in the target application. Additionally, the cell degradation dynamics need to be incorporated into the model. In order to account for these issues, the identification model was augmented with one state - the cell capacity Q_{max}. This state has zero dynamics, and its change is only modeled by noise, wherefore it works in the way of the *Schmidt-Kalman Filter* (SKF); see, e.g., [YBD10] for reference. The state equations are then given in equation 2.14,

$$\begin{bmatrix} \dot{SOC}(t) \\ \dot{V}_1(t) \\ \dot{V}_2(t) \\ \dot{T}_{\mathrm{bat}}(t) \\ \dot{Q}_{\mathrm{max}}(t) \end{bmatrix} = \begin{bmatrix} -\dfrac{I(t)}{Q_{\mathrm{max}}(t)} \\ \dfrac{I(t)}{\mathrm{C}_1} - \dfrac{V_1(t)}{\mathrm{R}_1\mathrm{C}_1} \\ \dfrac{I(t)}{\mathrm{C}_2} - \dfrac{V_2(t)}{\mathrm{R}_2\mathrm{C}_2} \\ \dfrac{V_1(t)I(t)}{\mathrm{C_{th}}} + \dfrac{V_2(t)I(t)}{\mathrm{C_{th}}} + \dfrac{R_0(SOC,\, T_{\mathrm{bat}})I(t)^2}{\mathrm{C_{th}}} + \dfrac{T_{\mathrm{air}}(t) - T_{\mathrm{bat}}(t)}{\mathrm{R_{th}\,C_{th}}} \\ 0 \end{bmatrix}. \tag{2.14}$$

The nonlinear dependencies for the internal resistance R_0 and open circuit voltage V_{OC} still hold as in equations 2.15 and 2.16,

$$R_0 = f_{R0}(\mathrm{SOC},\, T)\,, \tag{2.15}$$
$$V_{\mathrm{OC}} = f_{\mathrm{OCV}}(\mathrm{SOC},\, T)\,. \tag{2.16}$$

On the other hand, the model was shortened by one output - the SOC. As a result, there are only two outputs - the terminal voltage V_{trm},

$$V_{\mathrm{trm}} = V_{\mathrm{OC}} - V_2 - V_1 - R_0 I\,, \tag{2.17}$$

and the temperature T_{bat}. Together, they make up the output vector in equation 2.18,

$$y(t) = \begin{bmatrix} V_{\mathrm{trm}} \\ T_{\mathrm{bat}} \end{bmatrix}. \tag{2.18}$$

Chapter 3

Overview of SOC and SOH Estimation Methods

This chapter provides a brief overview of SOC and SOH estimation methods.

3.1 State of the Art - SOC Estimation

This section is mainly based on [HHA22]. A complete overview of SOC estimation methods is depicted in figure 3.1.

3.1.1 Coulomb counting (Ampere-hour Integral)

The first method for SOC determination mentioned in the literature, e. g. in [LHLZ17, BSM+20, Ple04b] and others, is the so-called *Coulomb counting* which is described by equation

$$SOC(t) = SOC_0 - \frac{\eta}{Q_{\max}} \int_0^t I(\tau)\, \mathrm{d}\tau\,, \tag{3.1}$$

where SOC_0 is the initial state, $Q_{\max}$ is the maximum currently available battery capacity, η is Coulombic efficiency, i is current that flows out from the battery and τ is time.

The main problem of this method is the necessity of precise knowledge of the initial condition and noiseless measurement. As the precise measurement is never truly available, regular calibration is inevitable. Moreover, this method cannot compensate for a battery self-discharge. Also, there is a large cumulative error.

3.1.2 Voltage measurement

There is a direct mapping from SOC to *Open Circuit Voltage* V_{OC}. This dependency could have a form of a look-up table, for example. Then, by measuring the V_{OC}, the SOC can be inferred directly. There are three major drawbacks. First, to measure the V_{OC}, the battery must be disconnected from the load, and it must rest for sufficiently long for all the transients to vanish. Second, some battery chemistries exhibit hysteresis in the V_{OC} -

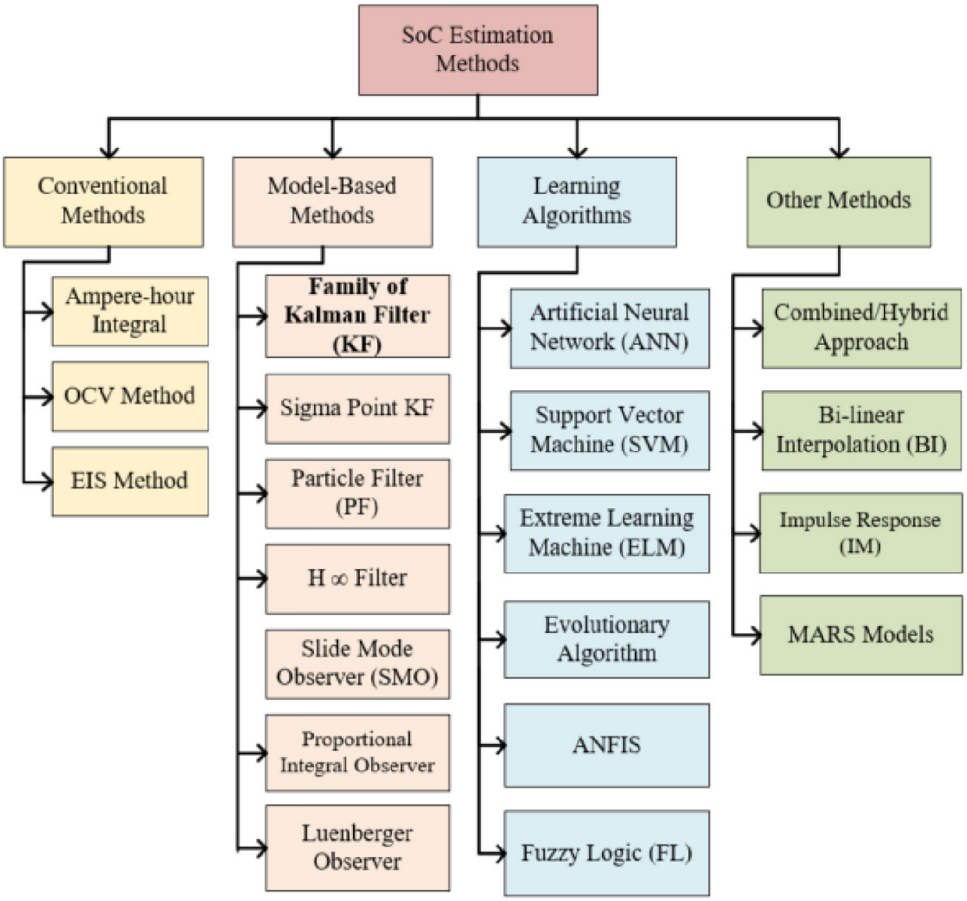

Figure 3.1: The family of SOC estimation methods. Source: [HHA22]

SOC dependence - different values for charging and discharging. Third, some battery chemistries have very flat regions of the function, which means that even a little change in the measured voltage means a big change in SOC. All things considered, this method is not suitable for applications where the highly dynamic loading of the battery is present. Also, the suitability of this method is not equal for all battery chemistry types.

3.1.3 Electrochemical Impedance Spectroscopy

The *Electrochemical Impedance Spectroscopy* (EIS) is able to capture several phenomena happening inside the cell ([WHS+18], [GP18]). The result is typically a Nyquist plot with distinct parts of characteristics related to inner electrochemical phenomena - a double-layer capacitance, charge transfer resistance at the electrode, diffusion effects of ions into the active material of the electrode, and phenomena occurring in places of contact of various electrical components of the cell. As a result, the EIS can provide high-precision data. On the other hand, creating a battery management system with EIS capability is expensive. Also, to fully exploit the information given by EIS, one must thoroughly understand electrochemical processes such as

ion conduction, diffusion, migration, charge transfer, and so on.

3.1.4 Machine Learning

The area of *machine learning* (ML) is vast, and there is a huge amount of methods that can be employed for SOC determination. Oftentimes, though, as the ML is able to supplement custom nonlinear mapping, these algorithms also typically estimate the *remaining useful life* (RUL), model parameters, and so on. Some of the techniques used in this area are: *artificial neural network* (ANN) [LPR+19], *adaptive neuro-fuzzy inference system* (ANFIS) [DGW+15], *support vector machine* (SVM) [AGd+13], fuzzy logic, *particle swarm optimization* (PSO) and others. As summarized in [HHA22], their advantages are typically the ability to work well for nonlinear systems - they achieve high accuracy. On the other hand, their main disadvantage is the need for a large amount of training and testing data and the computational expense.

3.1.5 Model-based Methods

The *model-based methods* (MBM) use a mathematical model, typically a set of algebraic-differential equations that exhibit behavior analogous to the real system in question. This model is embedded directly into the control algorithm. A distinct position among the MBM holds the numerous family of *Kalman Filters* (KF). However, apart from that, there are many other model-based estimation techniques: Luenberger observer, proportional-integral observer, sliding mode observer, particle filter [AW22], H-infinity filter [CSXH16], [YXL17], and moving horizon estimator [PBA14].

The best known optimal filter is *Linear Kalman Filter* (LKF). Compared to other filters, it has relatively low computational requirements. However, it is suited for linear systems. A battery cell is not a linear system. Thus, a relatively large estimation error must be accepted, or some ad-hoc linearization of the nonlinear part of the model must be carried out, as in [YHjX15].

The first alternative to LKF is *Extended Kalman Filter* (EKF). At the cost of increased computational effort, a smaller error can be achieved. In spite of the ad-hoc linearization of the model for use in the LKF, the EKF works universally. It is an approach widely used in the literature, for example, in the series of articles [Ple04a, Ple04b, Ple04c]. The EKF uses the first-order approximation to deal with the model nonlinearity.

As a further development of the aforementioned articles on EKF, articles [Ple06a] and [Ple06b] were created. They examine an approach fundamentally different from the EKF, the so-called *Sigma Point Kalman Filter* (SPKF). The SPKF does not carry out the first-order linearization. It describes the system states as probabilistic variables. There are two subtypes of SPKF mentioned - *Unscented Kalman Filter* (UKF) and *Central Difference Kalman Filter* (CDKF). The articles claim a superior performance of CDKF to EKF and [JZK18] privileges UKF to EKF.

3.2 State of the Art - SOH Estimation

The SOH is often being estimated in combination with SOC and other battery parameters, and thus the SOC and SOH estimation methods overlap. However, the SOH cannot be estimated by any equivalent to Coulomb counting or V_{OC} measurement, so the pool of SOH methods narrows down to model-based and machine learning (also called *data driven*) methods.

Regarding the model-based methods, there are several options for combining the SOC and SOH estimation. Firstly, the maximum available capacity Q_{max} can be included as a state in the system model. Such an approach was adopted in this thesis as it is the easiest and most straightforward way. Secondly, it can be estimated separately. For this purpose, there are multiple options from which to choose: recursive least squares and filters - Kalman, H-infinity... Some of the methods can be seen in [Ple06b], [PBA14], [AW22], [TKP15].

Chapter 4

Estimation Algorithm Implementation

It resulted from literature research that the EKF serves as a benchmark for all the model-based SOC and SOH estimation algorithms. Thus, it was implemented in this thesis, too, even though there are algorithms with reported better results.

4.1 Kalman Filtering

Loosely speaking, the Kalman filter is a clever way to combine system model and measurements to estimate the systems' states. It is assumed that both the system dynamics and measurements are subject to noise.

In the case considered in this thesis, the dynamic system in question is per se continuous, but it is assumed it has been discretized previously and that the measurements are discrete, too. The mathematical description goes as follows:

$$x_k = f_{k-1}(x_{k-1},\, u_{k-1},\, w_{k-1}), \tag{4.1}$$
$$y_k = g_k(x_k,\, v_k), \tag{4.2}$$
$$w_k \sim (0,\, Q_k), \tag{4.3}$$
$$v_k \sim (0,\, R_k), \tag{4.4}$$

where x denotes system states, $\dot{x}$ is differentiation of states according to time t, u denotes inputs and w is process noise. Furthermore, y_k stands for system output, $k = 1, 2, 3...$ are samples of discrete-time and v_k is measurement noise. Both the process and the measurement noise are random variables with zero mean and covariances given by Q and R. Also, they are by assumption mutually uncorrelated, white and Gaussian.

4.1.1 Algorithm

The incorporation of the system model and measurements into states and covariance propagation can be divided into two steps, called *time step* and *data step*. The discrete time is indicated by the lower index k, and the data step is indicated by the upper index plus (+) and minus (-). Also, the estimate

before the data step is called *a priori*, and after the data step, it is called *a posteriori*.

In the beginning, filter states and covariance must be initialized,

$$\hat{x}_0^+ = E(x_0), \qquad \text{and} \qquad P_0^+ = E[(x_0 - \hat{x}_0)(x_0 - \hat{x}_0)^T]. \tag{4.5}$$

It can be seen that the initial estimates are treated as being *a posteriori*. Henceforth, the states and covariance will be propagated through the system over the course of time. At each time step, the following partial derivative is evaluated:

$$A_{k-1} = \left.\frac{\partial f_{k-1}}{\partial x}\right|_{\hat{x}_{k-1}^+}. \tag{4.6}$$

It is a first-order approximation of the nonlinear state function f. The time step is then

$$P_k^- = A_{k-1} P_{k-1}^+ A_{k-1}^T + Q_{k-1}, \tag{4.7}$$
$$\hat{x}_k^- = f_{k-1}(\hat{x}_{k-1}^+, u_{k-1}, 0). \tag{4.8}$$

After that, a partial derivative

$$C_k = \left.\frac{\partial g_k}{\partial x}\right|_{\hat{x}_k} \tag{4.9}$$

is computed and then the data step can be performed.

$$L_k = P_k^- C_k^T (C_k P_k^- C_k^T + R_k)^{-1} \tag{4.10}$$
$$\hat{x}_k^+ = \hat{x}_k^- + L_k[y_k - g_k(\hat{x}_k^-, 0)] \tag{4.11}$$
$$P_k^+ = P_k^- - L(C P_k^- C^T + R) L^T \tag{4.12}$$

4.2 Implementation

The algorithm was implemented in MATLAB® environment using the matlab.System class which enables a great interconnection to MATLAB System Block in Simulink®. This framework is directly adjusted for dynamic systems' modeling, simulation, and subsequent code generation. The MATLAB System Block can be executed in two regimes - Code execution and Interpreted execution. The first one is fast, and the second one can be debugged step by step. However, the Code generation mode does not support some functionalities (e. g. storing function handles as object properties) that would come in handy during the implementation. As a result, several inevitable clumsy workarounds were made. After all, though, the MATLAB System class and block appeared as a suitable way for filter implementation.

The application-oriented model (equations 2.14 - 2.18) was used.

4.2.1 Discretization

In this thesis, the Kalman Filter is implemented in its discrete form. Therefore, the battery model must be discretized. For this purpose, the simple forward Euler method was utilized,

$$x_k = x_{k-1} + Ts \cdot f(x_{k-1},\, u_{k-1})\,, \tag{4.13}$$

where Ts is a discretization step. With respect to the prospective embedded application, the discretization step is $Ts = 0.01$ s. This is the frequency of CAN bus in the car.

4.2.2 Jacobian Matrix Computation

In each step of the filtering algorithm, states, inputs, and outputs are scaled in the first place (that appeared necessary to prevent numerical issues). Then, in the time step, the nonlinear states' function is approximated by a derivative which is obtained by numerical differentiation, more precisely by the *finite difference* method. This way, the matrix A in 4.6 is obtained. The perturbation size in the finite difference algorithm is constant, which is why proper scaling is so important. The equations 4.7 and 4.8 are computed. The time step is followed by the data step, where a finite difference differentiation is used once again to get the C matrix from equation 4.9. After that, the computation of equations 4.10, 4.11, and 4.12 follows.

The finite difference method approximation is computed according to equation 4.14,

$$f'(x) \approx \frac{f(x+h) - f(x)}{h}\,, \tag{4.14}$$

which comes from the definition of a derivative, equation 4.15,

$$f'(x) = \lim_{h \to 0} \frac{f(x+h) - f(x)}{h}\,. \tag{4.15}$$

The letter h denotes the perturbation. The equations 4.14 and 4.15 are written for scalar case. Since the model states are a 5-state vector, the differentiation algorithm must be adjusted accordingly. The states are perturbed one by one, and the division 4.14 yields a 5-by-1 vector in each iteration; this vector shows how a perturbation in one state (respective to the iteration) influences all the system states. In the end, a 5-by-5 matrix A is obtained.

Other differentiation methods that might come into consideration would be for example *symbolic differentiation* or *algorithmic differentiation*. The first one cannot be used because of the lookup tables present in the model. The second one is more involved than the finite difference method and would certainly bring an excessive computational burden. Nevertheless, it surely might be interesting to explore this option more in the future.

Chapter 5

Estimation Algorithm Validation

In this chapter, the implemented algorithm is tested. Two types of tests were made - with artificial simulation data and with data from a *Real Driving Experiment* (RDE). Because of that, this chapter starts with a description of the source of this RDE data - the formula car of the eForce FEE Prague Formula student racing team.

5.1 eForce Formula Car Description

Figure 5.1: eForce Formula Car Season 2021

In figure 5.1, the 11th generation of the formula car is shown. This car took part in the FS competition in season 2021.

For the purpose of this thesis, it is important to focus on powertrain systems. All units in the car communicate via CAN bus with a frequency of 100 Hz. The car is propelled by four independent in-hub motors. These

are excited by two inverters. The only source of energy for the whole car is a battery pack. A more detailed description of the battery and its electronics can be found in [Hai21].

5.2 Accumulator

The accumulator contains Melasta SLPBA942126 cells ([She19]) in a configuration 144s2p - 144 in series and 2 in parallel, divided into 9 stacks. The nominal voltage is 600 V, nominal energy is 14 Ah. Each stack is controlled by a *Battery Management System* (BMS). The BMS printed circuit board (PCB) uses the chip Texas Instruments q76PL455A-Q1. The BMS sends voltage and temperature data and also enables passive balancing. It subordinates to an *Accumulator Management System* (AMS). The AMS has several functions: it controls the *Accumulator Insulation Relays* (AIRs), which lay between electrodes of batteries and output terminals of the whole battery pack. It also controls the Precharge circuit, which prevents huge currents in the system during startup. It governs a Shutdown circuit, a safety feature that detaches the battery pack from the rest of the car in case of a malfunction or accident. It makes multiple voltage and current measurements. It takes care of communication. It also possesses an auxiliary power source for DC/DC converter startup.

The brain of the AMS is an STM32F105 microcontroller unit from ST Microelectronics. The currently used algorithm of SOC estimation works followingly: it models the battery pack as a real voltage source, i.e. an ideal voltage source in series with a resistor, and computes a voltage drop on this internal resistance and then directly infers on SOC from a previously determined look-up table. Also, it integrates instantaneous power at battery terminals and thus estimates energy drawn from the pack.

In figure 5.2, data from a Formula Student Endurance event were analyzed. As the current solution of the battery pack in the eForce formula car lacks active cooling, the temperature in the pack rises during the drive. Therefore, it is necessary to include thermal dynamics in the model.

5.3 Vehicle Dynamics Control Unit

Relatively to other electronic units, the *Vehicle Dynamics Control Unit* (VDCU) has the most computational power. Because of that, any computationally demanding algorithm, even for battery pack control, would be entrusted to VDCU and not to AMS. The microcontroller unit in the VDCU is a Texas Instruments TMS320F28377S chip which boasts a good digital signal processing performance.

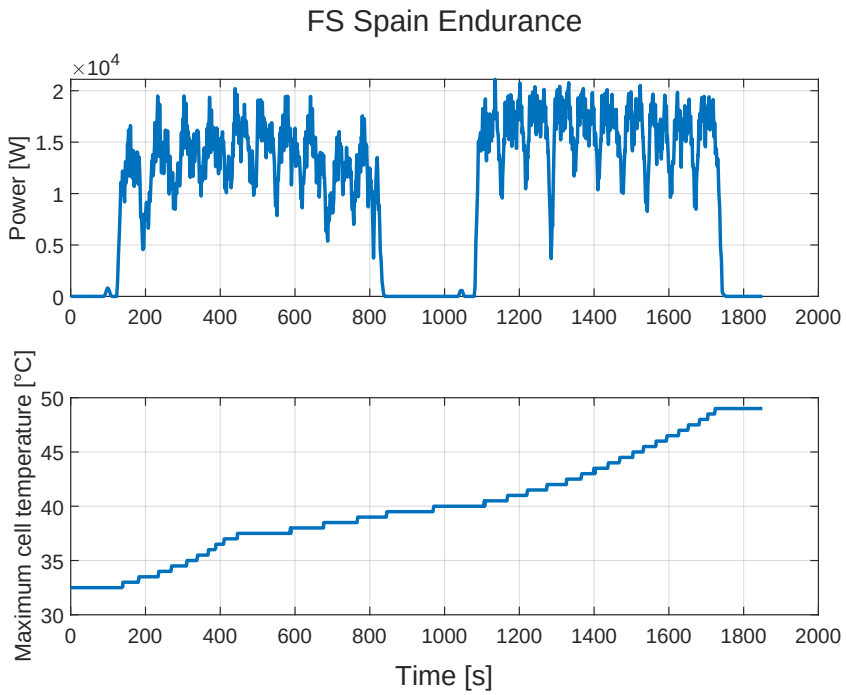

Figure 5.2: Power and temperature as output from battery pack

5.4 SOC Estimation Validation In Simulation

Firstly, the estimation algorithm is to be tested in a simulation environment. In the tests described below, the continuous model and the filter are compared.

5.4.1 Zero Input

The first experiment is the following: zero inputs and different initial conditions. Expected outcome: convergence of the states and outputs of the filter to that of the continuous model. The initial conditions are summarized in table 5.1 where CTM stands for *continuous time model* and KF stands for *Kalman filter*. The values in the middle two columns are scaled. Therefore there are the adjacent scaling constants stated in the last column.

State name	Initial Value CTM	Initial Value KF	Scaling
SOC	0.7	0	100
V_1	0	0	1
V_2	0	0	1
T_{bat}	0.5	0	65
Q_{max}	0.95	0.5	14

Table 5.1: Simulation Initial Values

Simulation results are shown in figure 5.3. The V_1 and V_2 states remained

zero for both the model and the filter, and the capacity $Q_{\max}$ unsurprisingly did not have any chance to converge to the model value of $Q_{\max}$, so it stayed at its initial value.

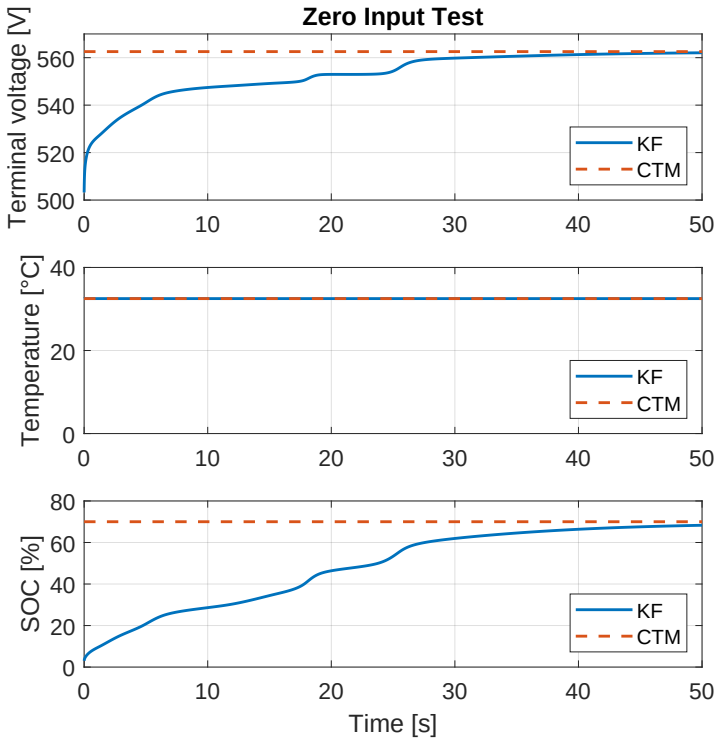

Figure 5.3: Simulation results for zero input

5.4.2 Constant Nonzero Input

This time, the initial conditions are the same for the continuous-time model, but changed for the filter to [1; 0.5; 0.5; 0.9; 0.95] (downscaled). The inputs are 50 A, and 20 °C. The simulation result is shown in figure 5.4.

It can be noted that the measured temperature converges instantly to model values. On the other hand, the SOC and the terminal voltage converge more slowly. That is also heavily affected by the time constants of the model.

5.4.3 Sine Sweep Input

The next experiment was done with [1; 0.5; 0.5; 0.9; 0.95] filter initial states' values and [100; 5; 5; 65; 14] scaling with the continuous-time model initial states being the same as in the preceding cases. The temperature input was constant at 20 °C. The current input performed a sweep from 0 to 5 Hz with 30 A amplitude and 30 A bias (so the wave oscillates between 0 and 60 volts). These values were chosen based on 2.4 and 2.9.

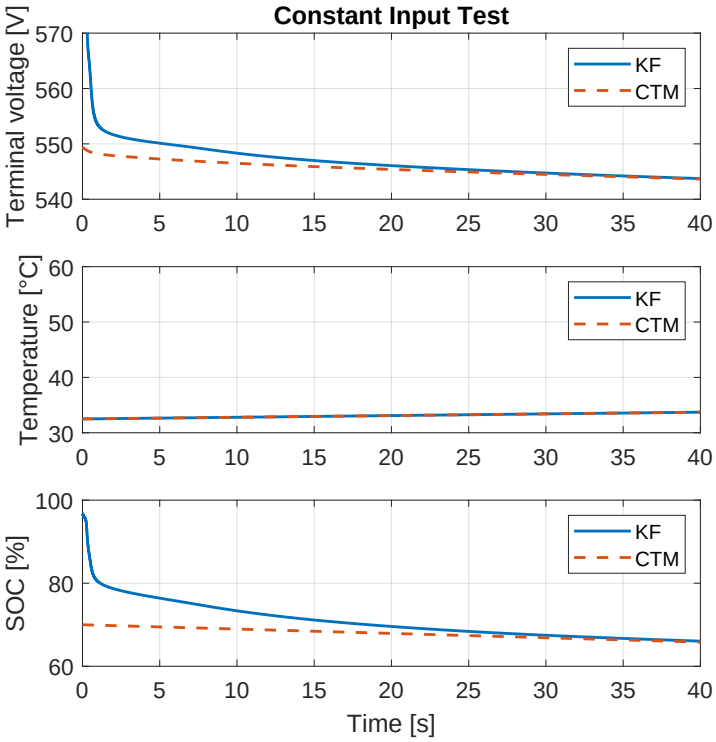

Figure 5.4: Simulation for constant input 50 A, 20 °C

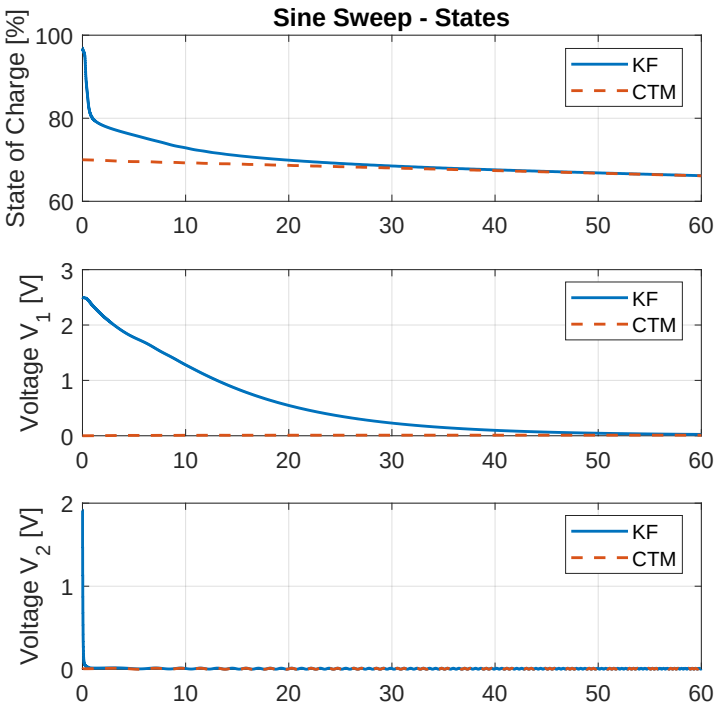

Figure 5.5: Sine Sweep Input, 0-60 A, 0-5 Hz

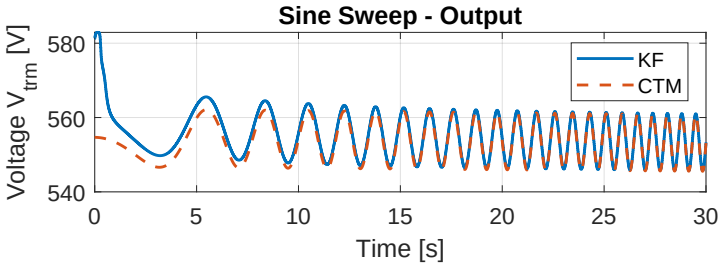

Figure 5.6:

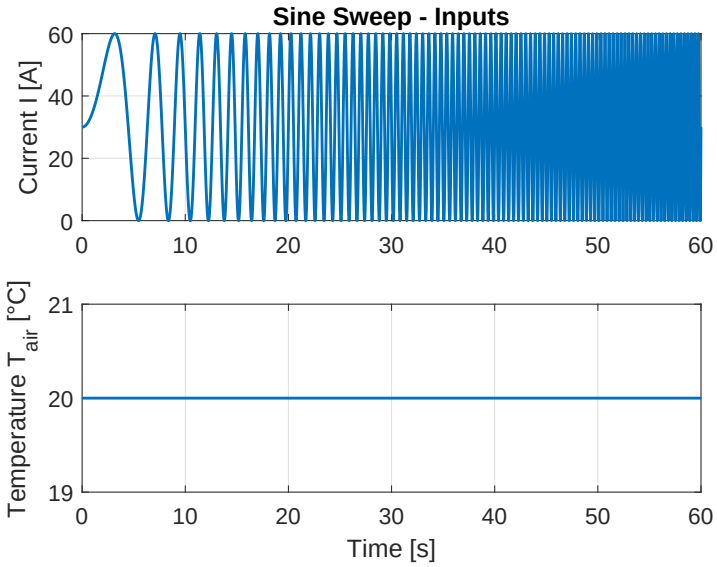

Figure 5.7:

The filter algorithm exhibits a convergence of the filter SOC value to that of the continuous-time model under 30 seconds, as depicted in figure 5.5.

5.5 SOC Estimation Validation with Experimental Data

The filter was tested not only against artificial simulation data but also against data taken during a *Real Driving Experiment* (RDE). The data used in the following test were collected during the Formula Student Spain 2021 Endurance event (so it is a different data set than the one used for model identification). Five signals are taken from the RDE data: the inputs Battery Terminal Current and Ambient Temperature that are shown in figure 5.8, the outputs Terminal Voltage and Battery Temperature, and one state, the SOC estimated by the then-used method.

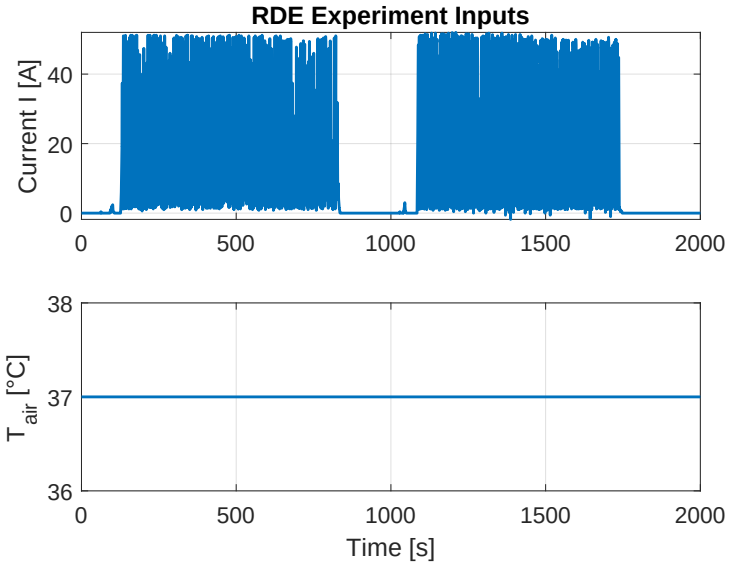

Figure 5.8: Inputs extracted from the RDE data

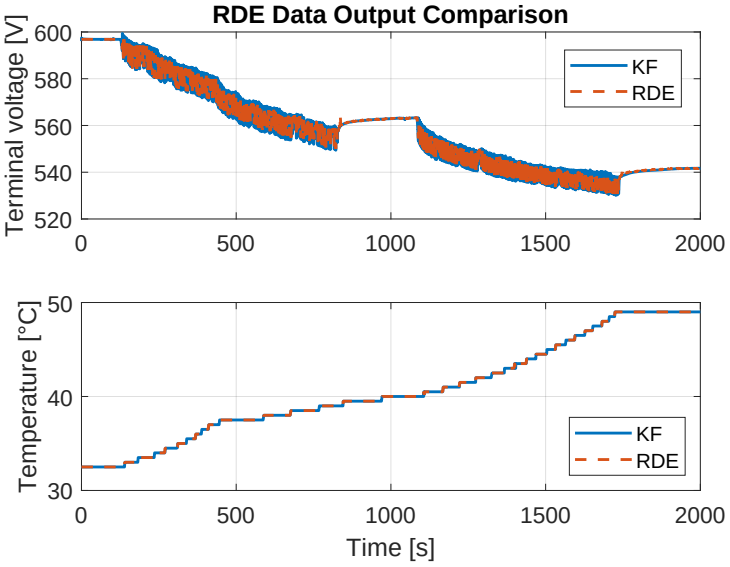

Figure 5.9: Output Comparison for RDE Input

In figure 5.9, the filter output terminal voltage and battery temperature are compared to the RDE terminal voltage and battery temperature. It can be seen that the data overlap - they overlap completely in the case of the second output (temperature) and somewhat less for the first output.

The figure 5.10 depicts an excerpt of several signals from between 300 s and 400 s of simulation time.

One of the descriptors that can be used for algorithm evaluation is *Root Mean Square Error* (RMSE). The RMSE of the terminal voltage signals is

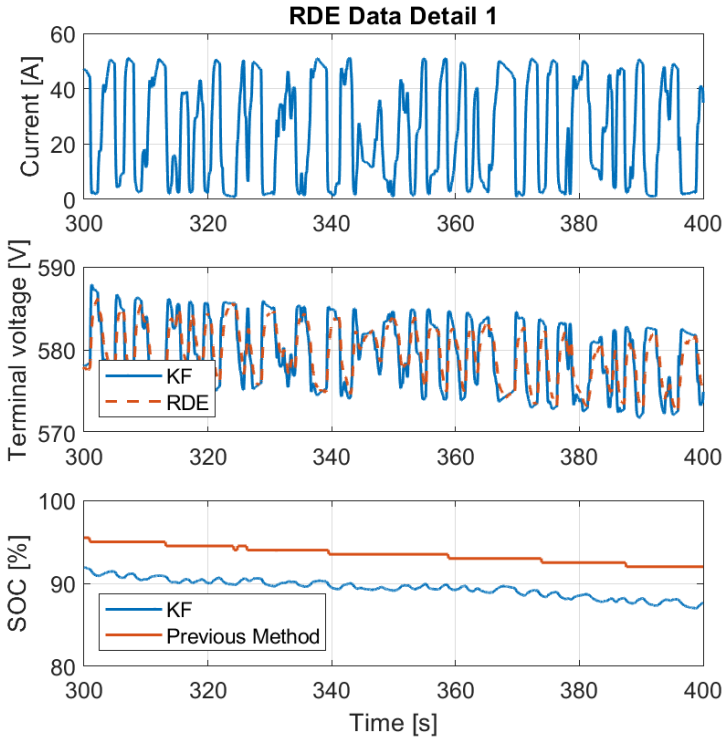

Figure 5.10: A detailed look at a part of the simulation data

given as

$$RMSE = \sqrt{\frac{\sum_{i=1}^{N} \left(V_i^{KF} - V_i^{RDE}\right)^2}{N}}, \tag{5.1}$$

where N is a number of samples, V^{KF} is a terminal voltage signal streaming from the filter, and V^{RDE} is battery terminal voltage coming from the real driving data. The value of the root mean square error is $RMSE = 1.54$ V, which is roughly 0.26 % of the maximum value of 600 V.

In figure 5.11, states of the filter and of the continuous-time model (both fed by the RDE inputs) are compared. The V_1 and V_2 voltages of the model's RC elements exhibit a decent overlap with RMSE equal to 0.12 V for both of them. The last state is the battery capacity $Q_{\max}$. It is also influenced by the tuning of Q and R matrices. Increasing the weight of the model provides better results under dynamic load. On the other hand, if the measurements are regarded as more important, it improves behavior in a steady-state (after the open-circuit voltage settles). Thus, smaller error in the dynamic part typically causes larger error in the steady-state and vice versa.

It can be seen in the lower graph of figure 5.10 that the filtered signal catches noise. However, the peak-to-peak value is usually around 0.7 percentage points. In other words, it has low significance.

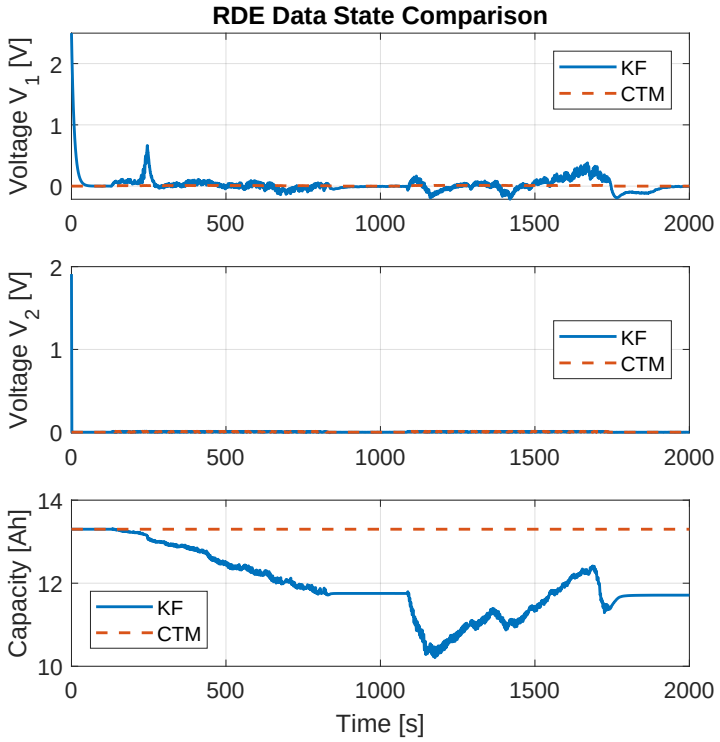

Figure 5.11: States Comparison for RDE Input

The presence of noise in the SOC filtered signal is directly connected to the ability of the filter to follow the terminal voltage. These effects counteract each other (*waterbed effect*), so a balance must be found. This behavior can be controlled by tuning the adjacent coefficients in covariance matrices Q and R in equations 4.3 and 4.4. For example, dividing the Q(1, 1) element by 10 lowers the value of the peak-to-peak oscillation to ca. 0.2 percentage point. However, the RMSE of output terminal voltage increases to 1.59 V. On the other hand, multiplying the original value of Q(1, 1) by 10 results in higher SOC peak-to-peak value, around 1.5 p. p., and lower voltage RMSE, 1.41 V.

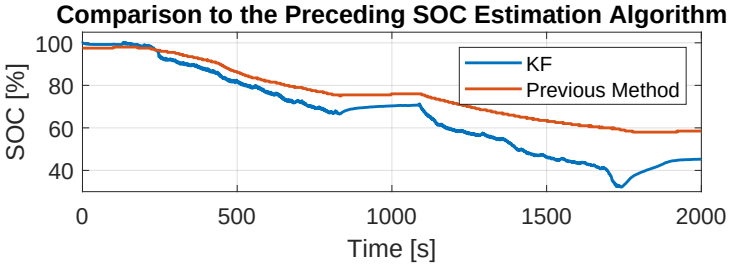

Figure 5.12: Old and new SOC estimation

In figure 5.12, two SOC estimation algorithms are compared to each other. It can be seen that the filter starts from perturbed initial conditions. Those

are the same as in the above described cases. The two algorithms present significantly different results. Their endpoints are 58.5% for the legacy algorithm and 45.2% for the new algorithm, which makes a 13.3 percentage points difference at the end of the run. The RMSE is 9.94 percentage points (p. p.). At this point it is worthy to remind the way the previous SOC estimation algorithm works. It models the battery as a real voltage source and uses a constant pre-determined internal resistance value and the measured current to compute the voltage drop over the internal resistance. After that, it calculates the open circuit voltage as a difference between the measured terminal voltage and the voltage drop. In the last step, it determines the SOC from an SOC - open circuit voltage look-up table. However, this look-up table was only guessed, not measured. The performance of the algorithm was improved by a digital filter based on real driving experiments. Computing the energy drawn from the battery pack is done via instantaneous power integration. These things considered, the previously used algorithm does not appear to be a reliable estimator. The newly implemented EKF-based algorithm utilizes truly measured SOC - OCV dependence and internal resistance dependence, the system's model covering two electrical dynamics and one thermal dynamic and even estimating the battery capacity. Moreover, there is the Coulomb counting method naturally embedded in the filter. Based on that, a conclusion can be stated that the new algorithm deserves more trust. Actually, under such circumstances, the inclusion of the previously estimated SOC into the identification process might be abandoned in the future.

Another interesting system's behavior is observed in the middle and at the end of the data signal. The two plateaus correspond to the change of drivers (as prescribed by the Formula Student rules) and to the end of the race. The filter algorithm claims the SOC rises in these moments. The open-circuit voltage rises, too. That can be seen in more detail in the snapshot of the middle plateau in figure 5.13. Taking common sense into account, this cannot be true because the terminal current is zero and so are voltages V_1 and V_2. Therefore, the increase in SOC must be a consequence of the unmodelled dynamics. That would justify the introduction of the third RC element into the model. Such an RC element would then have the longest time constant (the slowest dynamic) and would prevent the filtered SOC from rising.

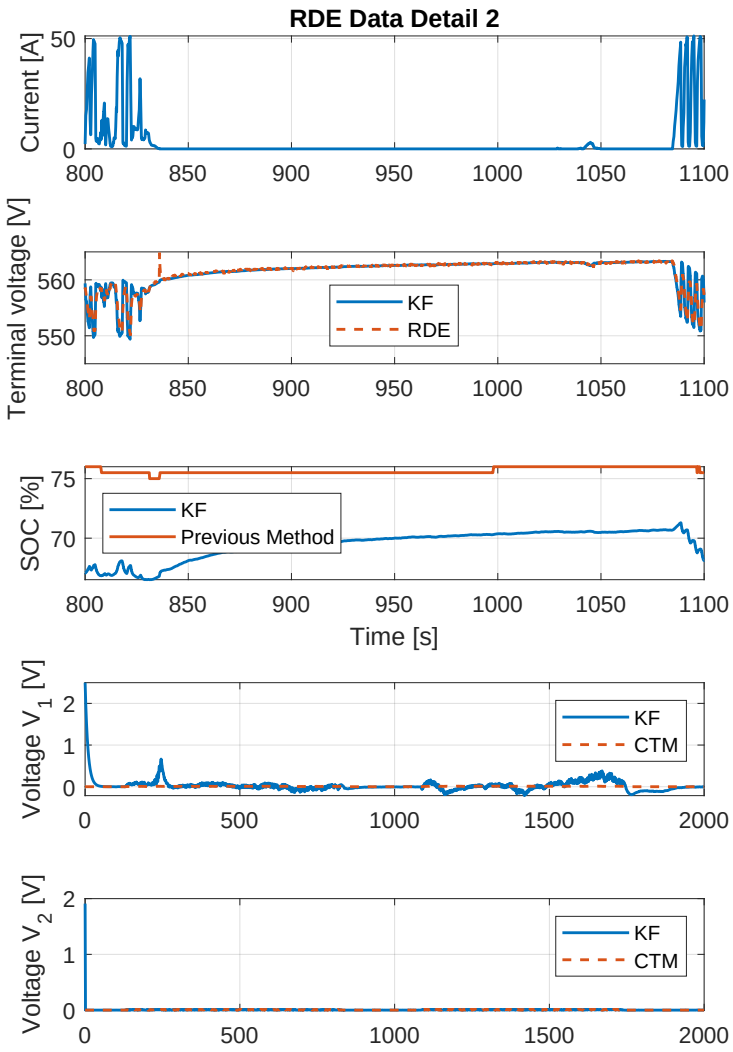

Figure 5.13: A detailed look at the phenomena occurring during the driver change

5.6 SOH Estimation Validation in Simulation

In order to test the algorithm's ability to estimate the SOH, a self-standing experiment was arranged where the filter is against compared to the continuous-time model. It was not possible to make an RDE experiment for SOH validation.

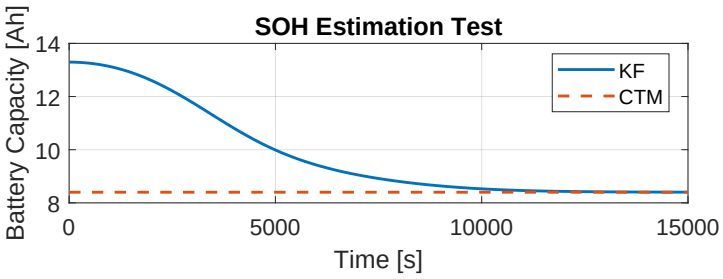

Figure 5.14: Comparison of filter and model capacity

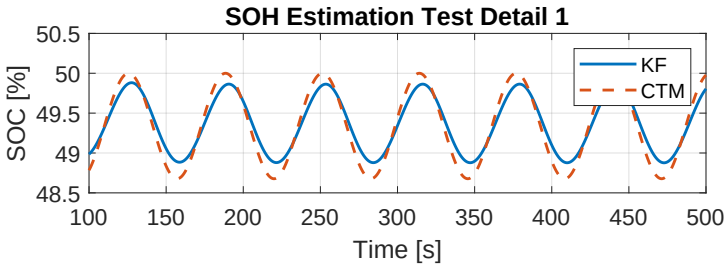

Figure 5.15: Filter and model SOC at the beginning of the simulation

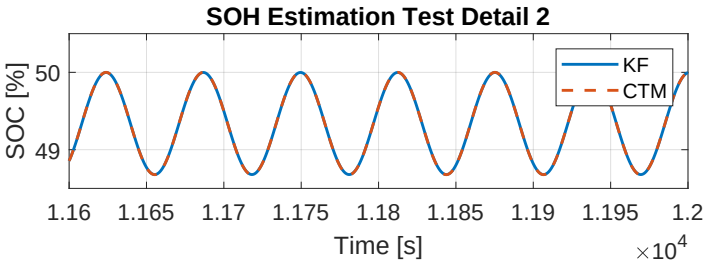

Figure 5.16: Filter and model SOC at the end of the simulation

To the input, a terminal current sine wave and constant ambient temperature were brought. The sine wave had an amplitude of 20 A and 0 bias and a frequency of 0.1 radians per second. Thus, the battery is both discharged and charged during the test, and the SOC remains close to its initial value. The initial states are set to [0.5; 0; 0; 0.2; 0.6] for the continuous-time model and to [0.5; 0.5; 0.5; 0.2; 0.95] for the filter. The figure 5.14 shows the complete run of the experiment. There, the filter correctly converges from its erroneous initial value to the correct value represented by the continuous-time model. The convergence takes approximately 2 hours and 45 minutes. The figure 5.15 shows the beginning of the test, and there it can be seen that the filter is not successful in tracking the CTM because of the incorrect value of battery capacity. On the other hand, the figure 5.16 exhibits the SOC values at the end of the test, and it can be observed that this time the signals are perfectly overlapped thanks to the correct value of the battery capacity.

Chapter 6

Conclusion

In this thesis, the usage of an Extended Kalman Filter for State of Charge and State of Health estimation of a pack of lithium-polymer batteries was described. This approach was chosen based on literature research. Subsequently, a model of the battery pack was devised. The model parameters were partly measured and partly identified from previously gathered data. The filter algorithm was implemented. Finally, the filter was tested both with simulation data and real driving experiment data against the continuous-time model of the battery pack. The whole work has been done with a prospective embedded automotive application in mind. However, it has not been possible to test the algorithm deployed in a car so far. The validation experiments proved successful convergence of the filter for both the states and the outputs.

Future work will be focused on the deployment of the algorithm into an embedded controller. That means examining the computational power of the target microcontroller unit by profiling. Then, it must be ensured the filter will work reliably in single-precision arithmetic. Furthermore, the performance of the filter could be assessed either by real driving experiments or (preferably) by a lab experiment, for example, by a rest-bus simulation. Expanding on the topic, there are many other filter algorithms that could be implemented both from the family of Kalman filters and beyond.

Bibliography

[AGd+13] J.C. Alvarez Anton, P.J. Garcia Nieto, F.J. de Cos Juez, F. Sanchez Lasheras, M. Gonzalez Vega, and M.N. Roquenhi Gutierrez, *Battery state-of-charge estimator using the svm technique*, Applied Mathematical Modelling **37** (2013), no. 9, 6244–6253.

[AW22] Mohamed Ahwiadi and Wilson Wang, *An enhanced particle filter technology for battery system state estimation and rul prediction*, Measurement **191** (2022), 110817.

[Bea19] Kirby W Beard, *Linden's handbook of batteries, fifth edition; 5th ed*, McGraw-Hill Education, May 2019.

[BSM+20] H. Bouchareb, K. Saqli, N. M'Sirdi, M. Oudghiri, and A. Naamane, *Electro-thermal coupled battery model: State of charge, core and surface temperatures estimation*, ICEERE2020 2nd International Conference on Electronic Engineering and Renewable Energy (Saidia, Morocco), April 2020, Available at `https://hal.archives-ouvertes.fr/hal-02486440`.

[Com14] International Electrotechnical Commission, *IEC 62620:2014 Secondary cells and batteries containing alkaline or other non-acid electrolytes - Secondary lithium cells and batteries for use in industrial applications*, 2014.

[CSXH16] Cheng Chen, Fengchun Sun, Rui Xiong, and Hongwen He, *A novel dual h infinity filters based battery parameter and state estimation approach for electric vehicles application*, Energy Procedia **103** (2016), 375–380, Renewable Energy Integration with Mini/Microgrid – Proceedings of REM2016.

[DGW+15] Haifeng Dai, Pingjing Guo, Xuezhe Wei, Zechang Sun, and Jiayuan Wang, *Anfis (adaptive neuro-fuzzy inference system) based online soc (state of charge) correction considering cell divergence for the ev (electric vehicle) traction batteries*, Energy **80** (2015), 350–360.

[Ele19] Elektro-Automatik GmbH, *Operating manual el 9000 b hp*, 8 2019, Available at `https://elektroautomatik.com/shop/media/pdf/20/36/25/33200700_EN.pdf`.

[GP18] Arijit Guha and Amit Patra, *Online estimation of the electrochemical impedance spectrum and remaining useful life of lithium-ion batteries*, IEEE Transactions on Instrumentation and Measurement **67** (2018), no. 8, 1836–1849.

[Groa] Boston Consulting Group, https://www.bcg.com/publications/2018/future-battery-production-electric-vehicles.

[Grob] ———, https://www.bcg.com/publications/2017/energy-environment-how-batteries-and-solar-power-are-disrupting-electricity-markets.

[Hai21] Petr Hainc, 2021, Available in Czech at `https://dspace.cvut.cz/handle/10467/95443?locale-attribute=en`.

[HHA22] M. Hossain, M.E. Haque, and M.T. Arif, *Kalman filtering techniques for the online model parameters and state of charge estimation of the li-ion batteries: A comparative analysis*, Journal of Energy Storage **51** (2022), 104174.

[HLP12] Xiaosong Hu, Shengbo Li, and Huei Peng, *A comparative study of equivalent circuit models for li-ion batteries*, Journal of Power Sources **198** (2012), 359–367, Available at `https://www.sciencedirect.com/science/article/pii/S0378775311019628`.

[jLhPK16] Hyun jun Lee, Joung hu Park, and Jonghoon Kim, *Comparative analysis of the soh estimation based on various resistance parameters for licoo2 cells*, 2016 IEEE Transportation Electrification Conference and Expo, Asia-Pacific (ITEC Asia-Pacific), 2016, pp. 788–792.

[JZK18] Ivan Jokić, Žarko Zečević, and Božo Krstajić, *State-of-charge estimation of lithium-ion batteries using extended kalman filter and unscented kalman filter*, 2018 23rd International Scientific-Professional Conference on Information Technology (IT), 2018, Available at `https://ieeexplore.ieee.org/document/8350462`., pp. 1–4.

[Key14] Keysight Technologies, *Keysight models 664xa, 665xa, 667xa, 668xa, and 669xa gpib dc power supplies operating guide*, 12 2014, Available at `https://www.keysight.com/de/de/assets/9018-01422/user-manuals/9018-01422.pdf?success=true`.

[Key17] Keysight Technologies, *Battery testing application note*, 12 2017.

[LHLZ17] Zhe Li, Jun Huang, Bor Yann Liaw, and Jianbo Zhang, *On state-of-charge determination for lithium-ion batteries*, Journal of Power Sources **348** (2017), 281–301, Available at https://www.sciencedirect.com/science/article/pii/S0378775317302859.

[LPR+19] Massimiliano Luzi, Maurizio Paschero, Antonello Rizzi, Enrico Maiorino, and Fabio Massimo Frattale Mascioli, *A novel neural networks ensemble approach for modeling electrochemical cells*, IEEE Transactions on Neural Networks and Learning Systems **30** (2019), no. 2, 343–354.

[PBA14] B. Pattel, H. Borhan, and S. Anwar, *An evaluation of the moving horizon estimation algorithm for online estimation of battery state of charge and state of health*, Proceedings of the ASME 2014 International Mechanical Engineering Congress and Exposition (Montréal, Quebec, Canada), no. IMECE2014-37140, November 2014.

[Ple04a] Gregory L. Plett, *Extended kalman filtering for battery management systems of lipb-based hev battery packs: Part 1. background*, Journal of Power Sources **134** (2004), no. 2, 252–261, Available at https://www.sciencedirect.com/science/article/pii/S0378775304003593.

[Ple04b] _____, *Extended kalman filtering for battery management systems of lipb-based hev battery packs: Part 2. modeling and identification*, Journal of Power Sources **134** (2004), no. 2, 262–276, Available at https://www.sciencedirect.com/science/article/pii/S037877530400360X.

[Ple04c] _____, *Extended kalman filtering for battery management systems of lipb-based hev battery packs: Part 3. state and parameter estimation*, Journal of Power Sources **134** (2004), no. 2, 277–292, Available at https://www.sciencedirect.com/science/article/pii/S0378775304003611.

[Ple06a] _____, *Sigma-point kalman filtering for battery management systems of lipb-based hev battery packs: Part 1: Introduction and state estimation*, Journal of Power Sources **161** (2006), no. 2, 1356–1368, Available at https://doi.org/10.1016/j.jpowsour.2006.06.003.

[Ple06b] _____, *Sigma-point kalman filtering for battery management systems of lipb-based hev battery packs: Part 2: Simultaneous state and parameter estimation*, Journal of Power Sources **161** (2006), no. 2, 1369–1384, Available at https://doi.org/10.1016/j.jpowsour.2006.06.004.

[She19] Shenzhen Melasta Battery, *Product specification polymer li-ion battery 3.7v 7000mah 15c*, 10 2019.

[Son] Sony Corporation, *Lithium ion rechargeable batteries technical handbook*.

[TKP15] Shijie Tong, Matthew P. Klein, and Jae Wan Park, *On-line optimization of battery open circuit voltage for improved state-of-charge and state-of-health estimation*, Journal of Power Sources **293** (2015), 416–428.

[WHS+18] Qian-Kun Wang, Yi-Jun He, Jia-Ni Shen, Xiao-Song Hu, and Zi-Feng Ma, *State of charge-dependent polynomial equivalent circuit modeling for electrochemical impedance spectroscopy of lithium-ion batteries*, IEEE Transactions on Power Electronics **33** (2018), no. 10, 8449–8460.

[YBD10] Chun Yang, Erik Blasch, and Phil Douville, *Design of schmidt-kalman filter for target tracking with navigation errors*, 2010 IEEE Aerospace Conference, 2010, pp. 1–12.

[YHjX15] Zhihao Yu, Ruituo Huai, and Lin jing Xiao, *State-of-Charge Estimation for Lithium-Ion Batteries Using a Kalman Filter Based on Local Linearization*, Energies **8** (2015), 1–20, Available at `https://www.researchgate.net/publication/282462924`.

[YXL17] Quanqing Yu, Rui Xiong, and Cheng Lin, *Online estimation of state-of-charge based on the h infinity and unscented kalman filters for lithium ion batteries*, Energy Procedia **105** (2017), 2791–2796, Available at `https://doi.org/10.1016/j.egypro.2017.03.600`.

[YXT+21] Lei Yao, Shiming Xu, Aihua Tang, Fang Zhou, Junjian Hou, Yanqiu Xiao, and Zhijun Fu, *A review of lithium-ion battery state of health estimation and prediction methods*, World Electric Vehicle Journal **12** (2021), no. 3.